N69-38146
NASA CR-105980

Department of Electrical Engineering

THE APPLICATION OF SEMICONDUCTORS TO QUASI-OPTICAL AND WAVEGUIDE ISOLATORS FOR USE AT MILLIMETER WAVELENGTHS

by

R. E. Hayes
M. Kanda
G. Masclet
W. G. May

UNIVERSITY OF COLORADO
BOULDER, COLORADO

THE APPLICATION OF SEMICONDUCTORS TO QUASI-OPTICAL AND WAVEGUIDE ISOLATORS FOR USE AT MILLIMETER WAVELENGTHS

by

R. E. Hayes
M. Kanda
G. Masclet
W. G. May

July 1969

Prepared under Grant No. NGR06-003-088 by

Electrical Engineering Department
University of Colorado
Boulder, Colorado

for

Electronics Research Center

National Aeronautics and Space Administration

ABSTRACT

An experimental and theoretical investigation of the utilization of anisotropic effects in semiconductor plasmas for the development of millimeter wavelength isolators is described. The topics reported on include a study of a quasi-optical isolator that depends on Faraday rotation in indium antimonide and a study of a waveguide isolator employing several configurations of indium antimonide cylinders as a part of the guiding structure. All of the devices were operated at a frequency of 94 GHz and at a temperature of 75°K. Typical experimental results for the Faraday rotation devices was a forward insertion loss of about 1 db with an isolation of 9 db. Corresponding data for typical waveguide devices was about 2.5 to 5 db of forward loss and 20 to 30 db of isolation. It is concluded that devices of the type described here for operation in the millimeter wavelength range must be cooled. At higher frequencies this may not be necessary.

TABLE OF CONTENTS

PAGE

LIST OF SYMBOLS

B_o	=	longitudinal magnetic field
c	=	speed of light in vacuum
e	=	electron charge
m_o	=	free electron mass
m^*	=	effective mass of electron
n	=	electron density
α	=	real part of Γ
β	=	imaginary part of Γ
Γ	=	propagation constant
$\mathcal{E}$	=	ellipticity
ε	=	relative dielectric constant
ε'	=	real part of ε
ε''	=	imaginary part of ε
ε_ℓ	=	relative lattice dielectric constant
ε_o	=	free space permittivity
θ	=	Faraday rotation angle
μ	=	mobility
μ_o	=	free space permeability
$\underline{\underline{\sigma}}$	=	tensor conductivity
τ	=	collision time
ω_c	=	cyclotron frequency
ω_p	=	plasma frequency

1. INTRODUCTION

The purpose of the work described in this report is to investigate the utilization of anisotropic effects in a semiconductor plasma for the development of millimeter wavelength control devices such as isolators and circulators. The potential importance of nonreciprocal semiconductor devices is in the flexibility of design that comes with the wide range of semiconductor parameters that can be easily achieved, in the possible compatibility with other semiconductor devices, and also in the new geometrical configurations that result when the primary field that interacts with the material is the microwave electric field and not the microwave magnetic field as in the case of ferrites.

The topics which have been investigated include a study of a quasi-optical isolator that depends upon Faraday rotation in a semiconductor and a study of a waveguide isolator that employs semiconductor cylinders of several configurations as a part of the guiding structure. A previous report titled, "Nonreciprocal Semiconductor Millimeter Wave Devices", for this project summarized the initial results obtained on these topics. The present report brings to a close these efforts and presents the final data and conclusions for the quasi-optical and waveguide isolators for use at millimeter wavelengths. Subsequent efforts supported by this grant will be to extend component development into the far infrared portion of the spectrum.

2. QUASI-OPTICAL ISOLATORS AND CIRCULATORS

This work is being performed by G. Masclet and R.E. Hayes.

2.1 Introduction

The purpose of this project was to investigate the possible millimeter wave device applications of an electromagnetic plane wave propagating in a solid-state plasma in a magnetic field. The magneto-optical effect encountered is the so-called Faraday effect characterized by the rotation of the plane of polarization of an electromagnetic wave in the presence of a static longitudinal magnetic field. The Faraday effect measurements described here were performed using various samples of indium antimonide in liquid nitrogen at a frequency of 94 GHz. The structures employed were quasi-optical, i.e., they propagated an essentially plane wave.

Several workers have investigated the Faraday effect in various semiconductors but experiments were confined to guided electromagnetic waves [1-10]. A number of these experiments have used InSb because of its high mobility and small carrier concentration obtainable at liquid nitrogen temperature. [5-10]

In the first part of this report we consider briefly the free electron Faraday effect theories. The second part gives a description of the physical model used in the experimental investigation of the Faraday effect and the results obtained. The third part describes the nonreciprocal quasi-optical devices based upon the anisotropic conductivity tensor of the plasma, their behavior is presented and discussed.

2.2 Theoretical Results

General theories of the free carrier Faraday effect have been presented by many authors. [11-14] In the usual treatment, the rotation of the plane of polarization and the ellipticity of the transmitted radiation are derived without taking account of the waves reflected from the surfaces of the specimen. Donovan and Medcalf first gave a complete analysis including these multiple reflections. [15-16]

Choosing a reference system, as shown in Fig. 1, such that the direction of propagation of the electromagnetic wave as well as the direction of the static magnetic field be along the z-direction, then the x, and y components of the electric vector E of the electromagnetic wave are non-zero. The linearly polarized plane wave can be represented by clockwise and counter-clockwise circularly polarized waves of equal amplitude that can be defined as

$$E_{\pm} = E_x \pm jE_y \tag{2.1}$$

A solid state plasma is a highly conductive medium with a tensor conductivity governed by Maxwell's equations. This tensor has the form:

$$\vec{j} = \underline{\underline{\sigma}}\,\vec{E},$$

$$\begin{bmatrix} j_x \\ j_y \\ j_z \end{bmatrix} = \begin{bmatrix} \sigma_\perp & \sigma_x & 0 \\ \sigma_x & \sigma_\perp & 0 \\ 0 & 0 & \sigma \end{bmatrix} \begin{bmatrix} E_x \\ E_y \\ E_z \end{bmatrix}, \tag{2.2}$$

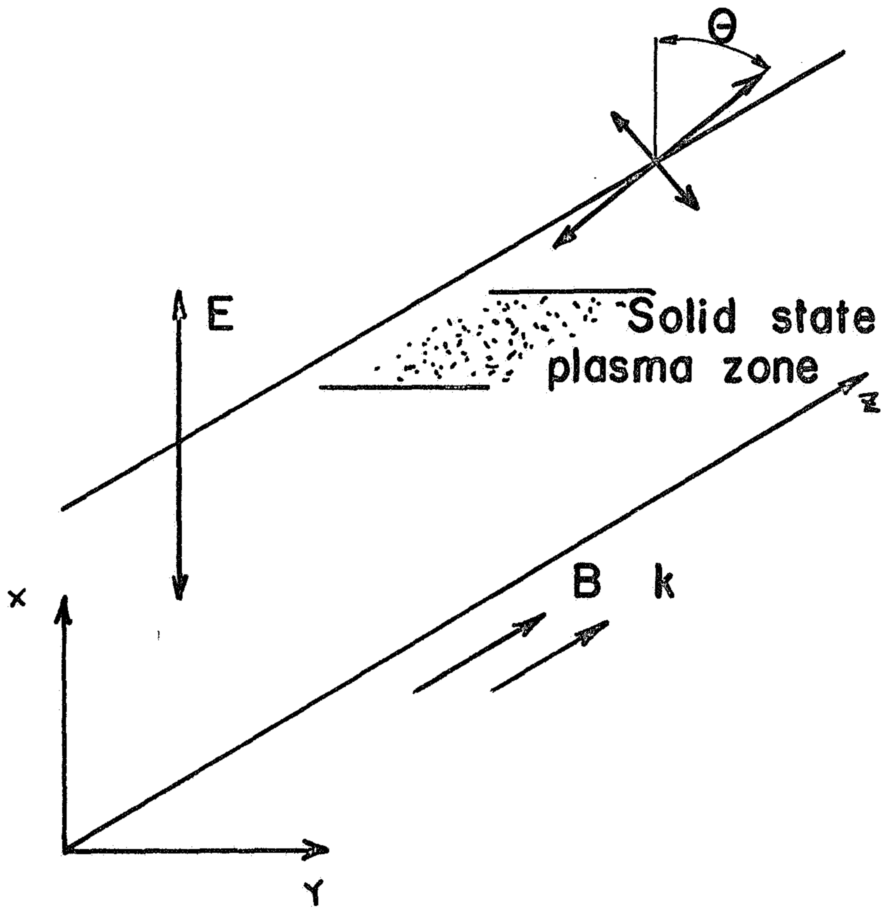

Figure I_ Faraday effect of a plane wave in a solid state plasma medium.

the two circularly polarized waves are then seen to propagate with a wave variation of the form $e^{(\Gamma z - j\omega t)}$ and with different propagation constants:

$$\Gamma_{\pm} = (\alpha_{\pm} + j\beta_{\pm}). \tag{2.3}$$

It can be shown that:

$$\Gamma_{\pm}^2 = -\omega^2 \varepsilon_{\ell} \mu_o \left[1 - \frac{j\omega_p^2 \tau}{\omega[1 + j\tau(\omega \pm \omega_c)]} \right] \tag{2.4}$$

Letting the static magnetic field be high enough so that we can write the following approximations,

$$\omega_c = \frac{\ell B_o}{m^*} >> \omega \quad ; \quad \omega_c \tau = \mu B_o >> 1 \quad ; \quad \omega\omega_c >> \omega_p^2 \; . \tag{2.5}$$

then the real and imaginary parts of the complex dielectric constants seen by each circularly polarized wave can be expressed as,

$$\varepsilon_{\pm}' = 1 - \frac{\omega_p^2}{\omega\omega_c} \tag{2.6}$$

$$\varepsilon_{\pm}'' = \frac{\omega_p^2}{\omega\omega_c^2 \tau} \tag{2.7}$$

The propagation constant for the clockwise polarized wave becomes,

$$\Gamma_{+} = \sqrt{\varepsilon_{\ell} \mu_o} \left[\frac{1}{2} \frac{\omega_p^2}{\tau\omega_c^2} + j\omega \left(1 - \frac{\omega_p^2}{2\omega\omega_c}\right) \right] \tag{2.8}$$

and for the counter clockwise,

$$\Gamma_- = \sqrt{\varepsilon_\ell \mu_o} \left[\frac{1}{2} \frac{\omega_p^2}{\tau \omega_c^2} + j\omega (1 + \frac{\omega_p^2}{2\omega\omega_c}) \right] . \tag{2.9}$$

The Faraday rotation of the plane polarized wave is caused by the difference in phase velocities of the two circularly polarized waves. The angle of such rotation per unit length is given by:

$$\Theta = \frac{1}{2} (\beta_+ - \beta_-) \quad . \tag{2.10}$$

The attenuation coefficients $\alpha_\pm$ define the ellipticity of polarization, i.e., the ratio of the minor axis to the major axis of polarization,

$$\mathcal{E} = \frac{1}{2} \tanh (\alpha_- - \alpha_+) \quad . \tag{2.11}$$

In the case of strong magnetic fields it is seen that the linearly polarized input wave will emerge also linearly polarized on the other side of the sample after undergoing Faraday rotation and being somewhat attenuated. It should be noted that if one of the attenuation constants is much greater than the other, e.g., $\alpha_+ >> \alpha_-$ then the emerging wave will be totally circularly polarized. The wave is then called a "helicon" wave. The elliptically polarized wave would be encountered for cases in between the two cited above.

In the above analysis there was no mention of the influence of multiple reflections at the boundaries of the solid state plasma. The effects of multiple reflections on the transmission properties of an infinite semiconductor sheet of finite thickness were derived by Donovan and Medcalf. [15,16]

In their analysis the portion of radiation transmitted into the semiconductor is also split into clockwise and counterclockwise circularly polarized components. The transmitted wave emerges in general, from the outer surface of the semiconductor, with elliptic polarization. Maxwell's equations are then solved to find the H fields from the stated E fields. The boundary conditions of continuous tangential E and tangential H are then applied to determine the reflection and transmission coefficients at the free space semiconductor boundary. The emerging fields are:

$$E_x = \frac{1}{2}E_o\left[K_+ \exp(-\Gamma_+ d) + K_- \exp(-\Gamma_- d)\right],$$

$$E_y = \frac{1}{2}E_o\left[K_+ \exp(-\Gamma_+ d) - K_- \exp(-\Gamma_- d)\right], \qquad (2.12)$$

where $K_{\pm} = K'_{\pm} + jK''_{\pm}$

also $$K_{\pm} = \frac{1+R_{\pm}}{1-R_{\pm}\exp(-2\Gamma_{\pm}d)} \qquad (2.13)$$

$$R_{\pm} = \left[\frac{\Gamma_{\pm}-j\omega/c}{\Gamma_{\pm}+j\omega/c}\right]^2 .$$

These results are derived by an infinite summing of the reflected and transmitted wave at the two boundaries. The expressions (2.12) and (2.13) can then be used along with the incident wave expression to derive the rotation and ellipticity formulas per unit length as:

$$\Theta = \frac{\beta_+ - \beta_-}{2} + \text{arc tan}\,\frac{K'_+K''_- - K'_-K''_+}{K'_+K''_- + K'_-K''_+} \tag{2.14}$$

and,

$$\mathcal{E} = \frac{|K_+|\exp(-\Gamma_+ d) - |K_-|\exp(-\Gamma_- d)}{|K_+|\exp(-\Gamma_+ d) + |K_-|\exp(-\Gamma_- d)}\ . \tag{2.15}$$

The loss through the sample is evaluated by taking the ratio of the squares of the amplitudes of the emerging wave to that of the incident wave. The resulting loss is given by:

$$\text{Loss} = -10 \log \left[|E_{xo}|^2 + |E_{yo}|^2\right] \tag{2.16}$$

These equations are exact expressions of the free carrier Faraday rotation and the ellipticity of the emerging wave transmitted through the semiconductor plasma with a conductivity matrix of the form given by (2.2). Thus the reflections occurring in the sample bring significant changes in the expression for the angle of the Faraday rotation and for the ellipticity of polarization of the generally elliptically polarized wave transmitted through the semiconductor plasma. These expressions are too complicated compared to the expressions given in (2.10) and (2.11) for practical computation without the aid of a computer.

Calculations were carried out for various parameters. Figures 2, 3, 4, 5 show the Faraday rotation and loss as a function of sample thickness for a magnetic field of 1Wb/m^2 and for several typical values of electron density and mobility.

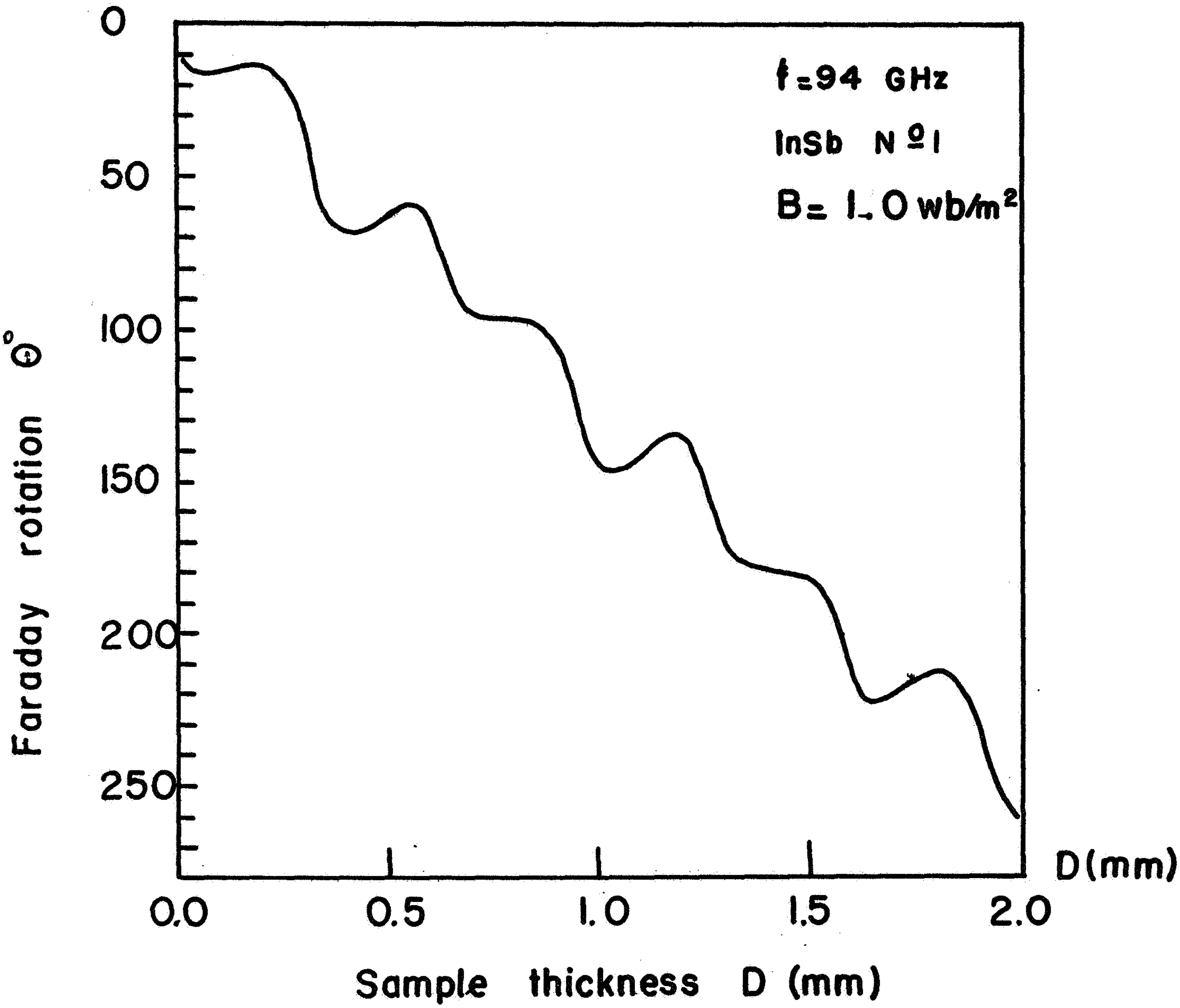

Figure 2 _ Calculated Faraday rotation

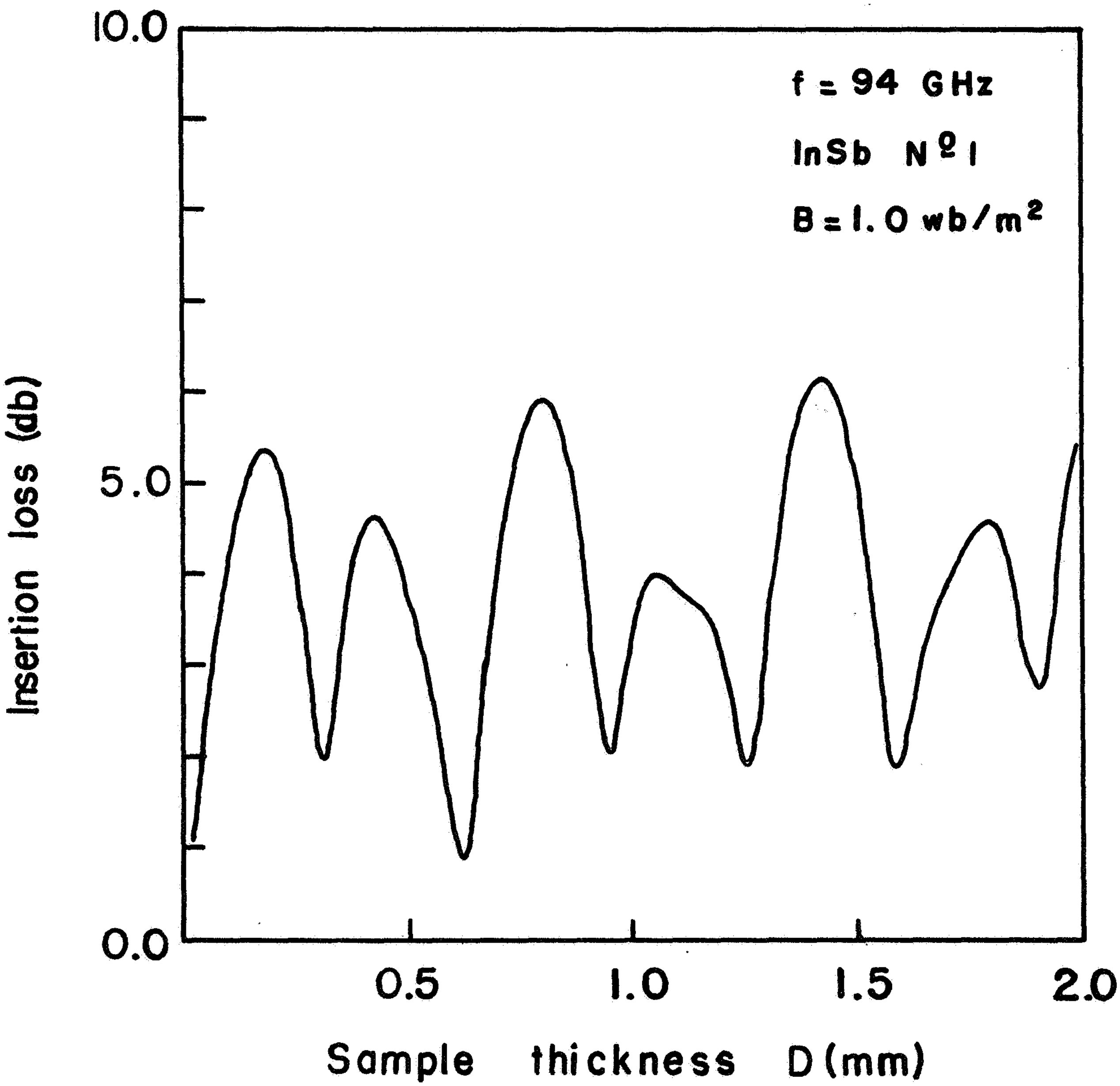

Figure 3_ Calculated insertion loss

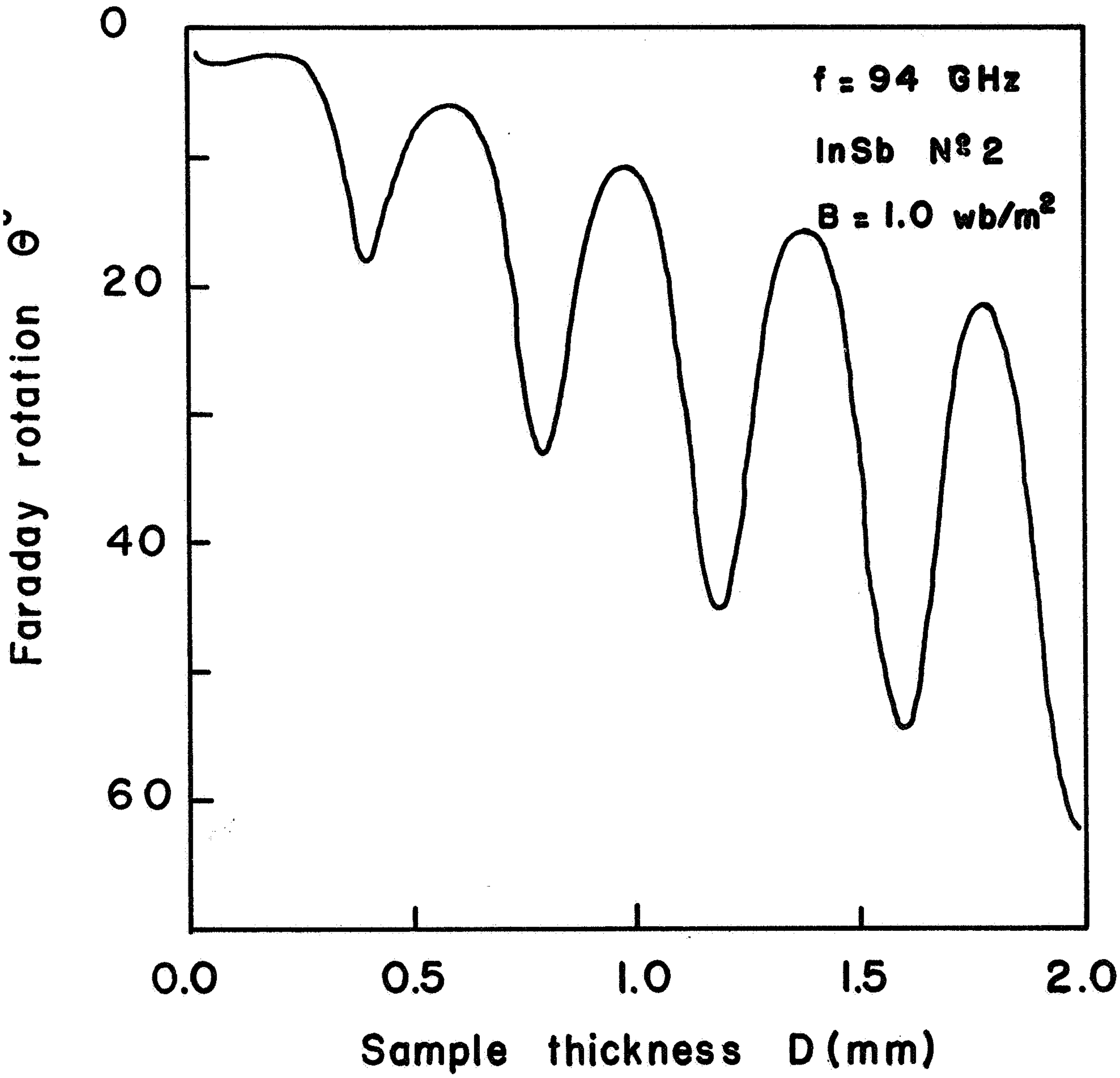

Figure 4 _ Calculated Faraday rotation

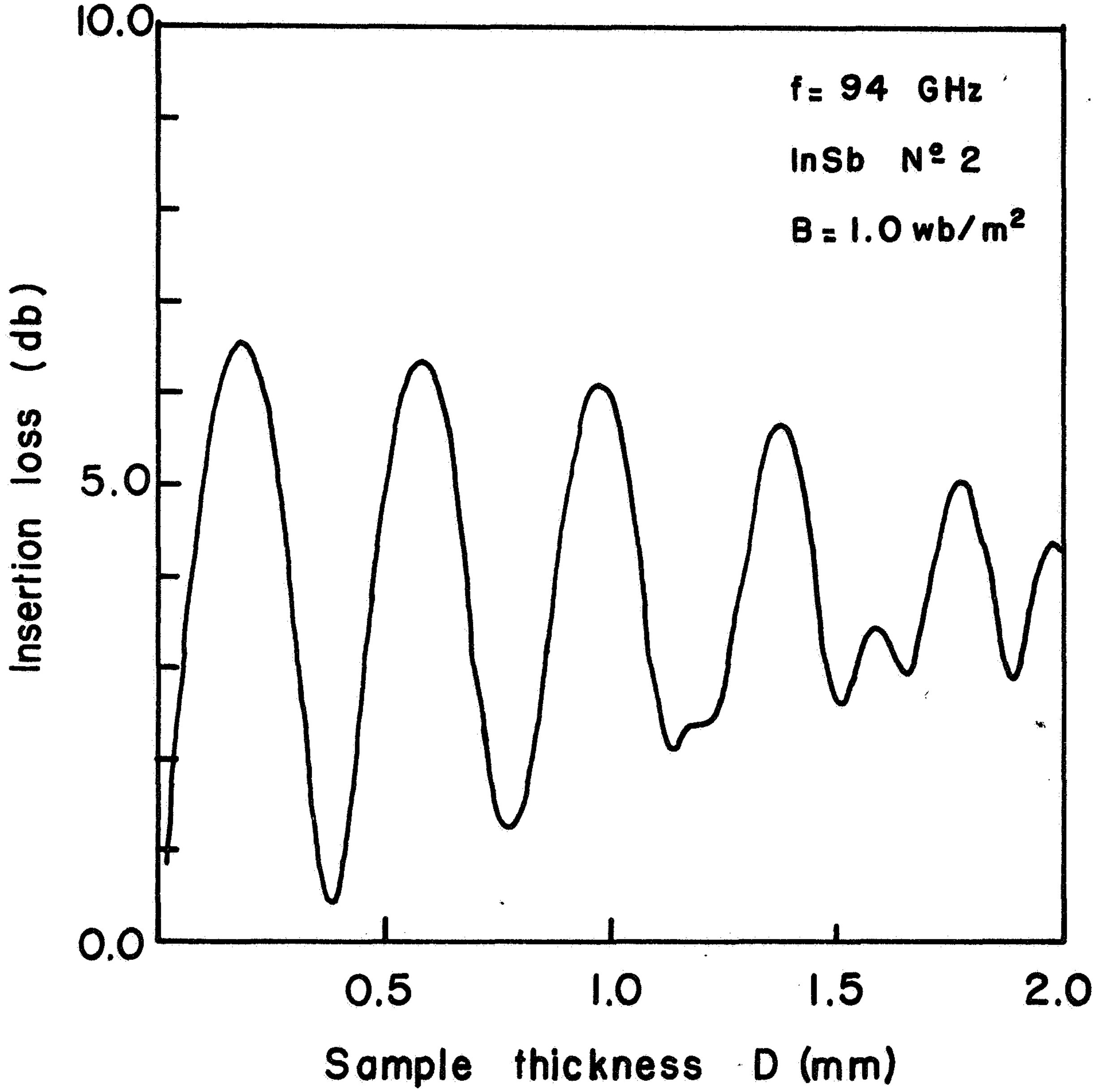

Figure 5 _ Calculated insertion loss

The parameters for sample number 1 are:

$$n = 2.8 \times 10^{14} cm^{-3},$$

$$\mu = 5.0 \times 10^{5} cm^{2}/v\text{-sec}.$$

The values for sample number 2 are:

$$n = 5.0 \times 10^{13} cm^{-3}$$

$$\mu = 3.5 \times 10^{5} cm^{2}/v\text{-sec}.$$

These results clearly exhibit the geometrical resonances encountered. Figures 6, 7 show the Faraday rotation and the loss as a function of magnetic field for the material parameters given in Figures 2 and 3, and for a thickness of 0.95mm.

2.3 Experimental Results

In this section we compare the experimental results with the theoretical predictions using Donovan and Medcalf's theory.

The experiments when chosen to be done at 94 GHz since this is a frequency of practical importance in the millimeter wavelength range.

The material selected was indium antimonide due to its high electron mobility but with relatively high resistivity in order to obtain the Faraday effect with small attenuation. The samples were cooled to liquid nitrogen temperature. They had the following characteristics which were measured by the Van der Pauw [17] technique rather than by the usual Hall method. The experimental setup to observe the Faraday effect was as shown in Figures 8 and 9. The horns were far apart so that the quasi-optical conditions were met. The receiving horn could be rotated so that the relative angle between input and output waveguides could be

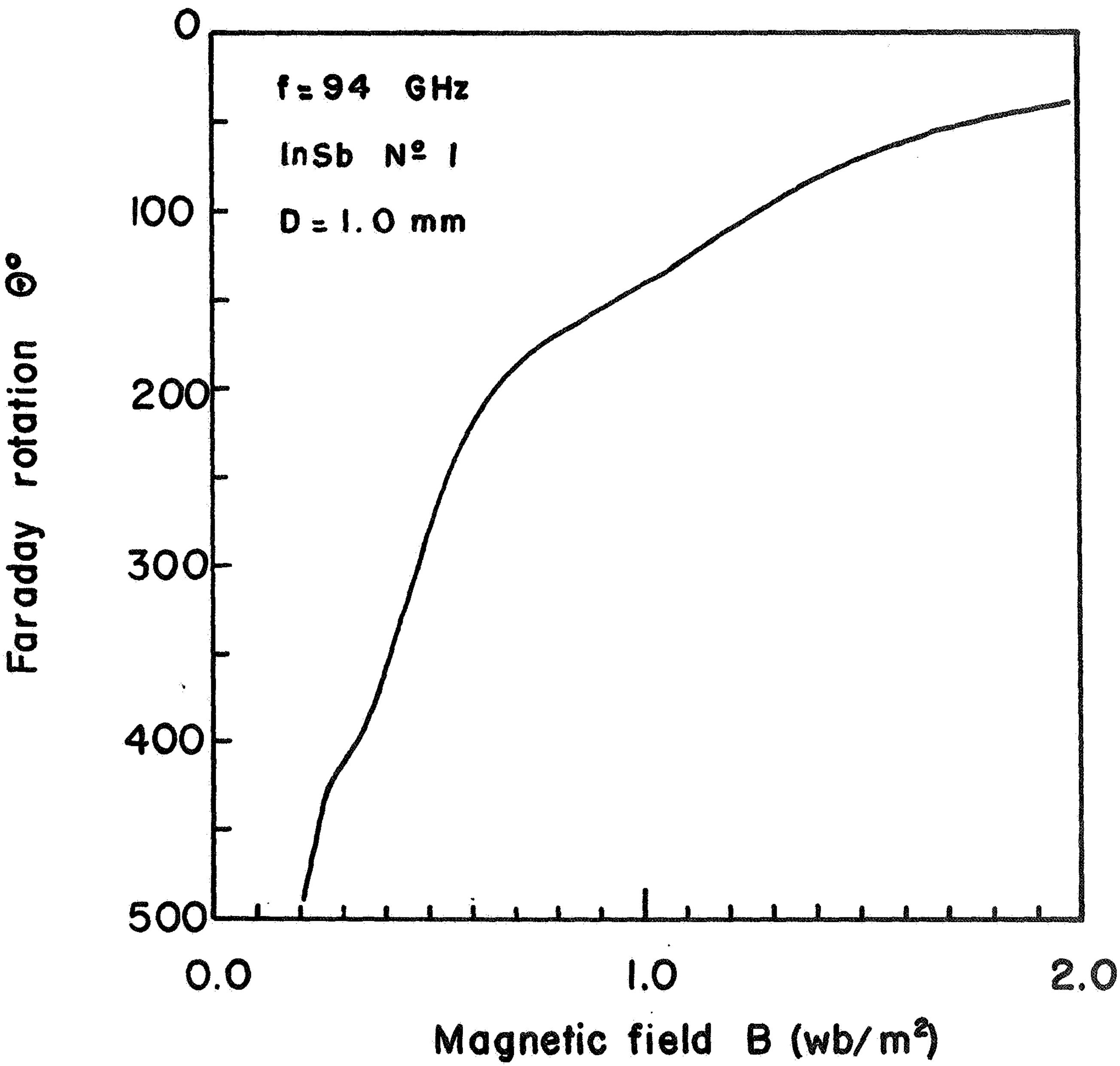

Figure 6 _ Calculated Faraday rotation Θ°

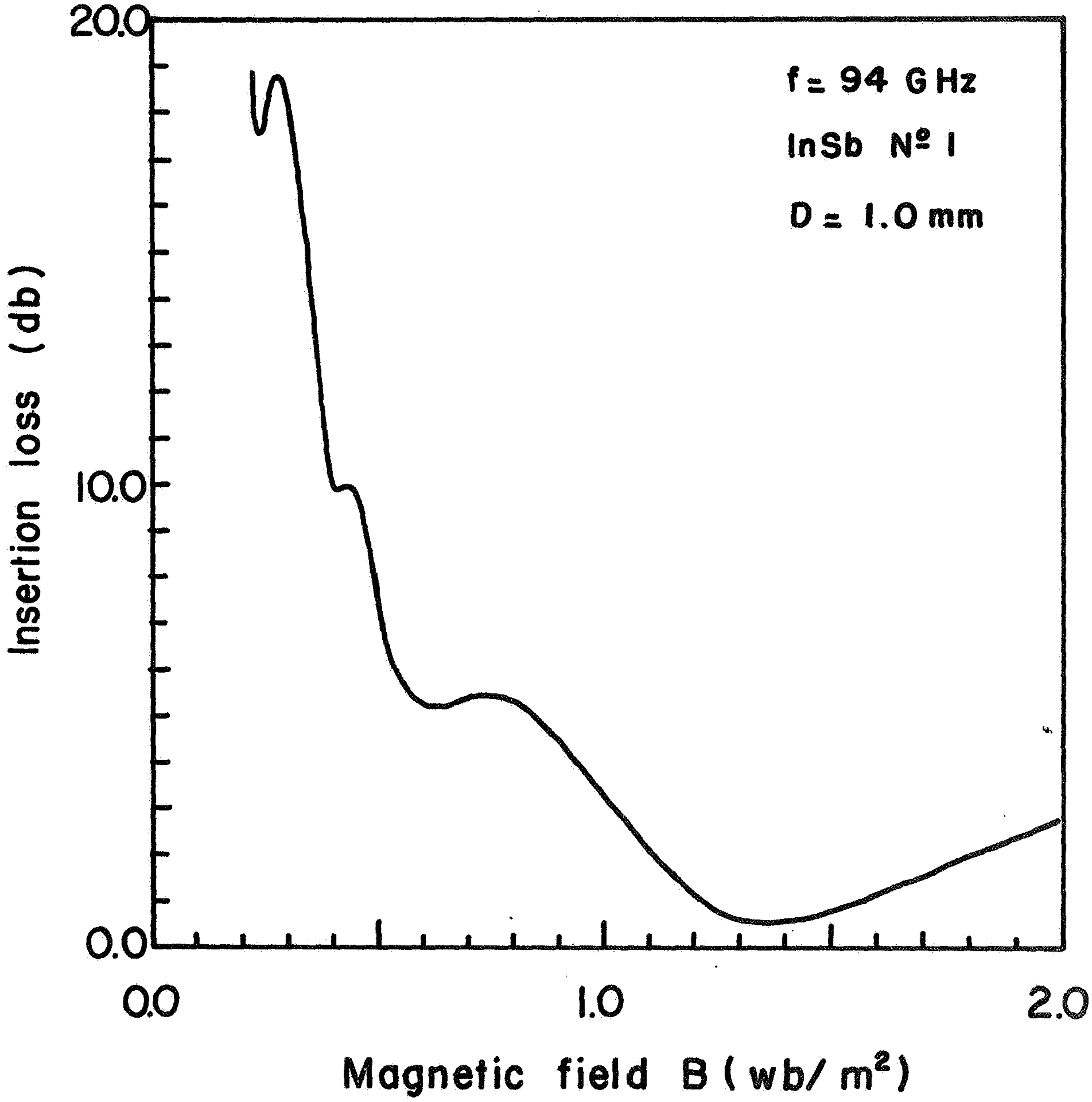

Figure 7 _ Calculated insertion loss (db)

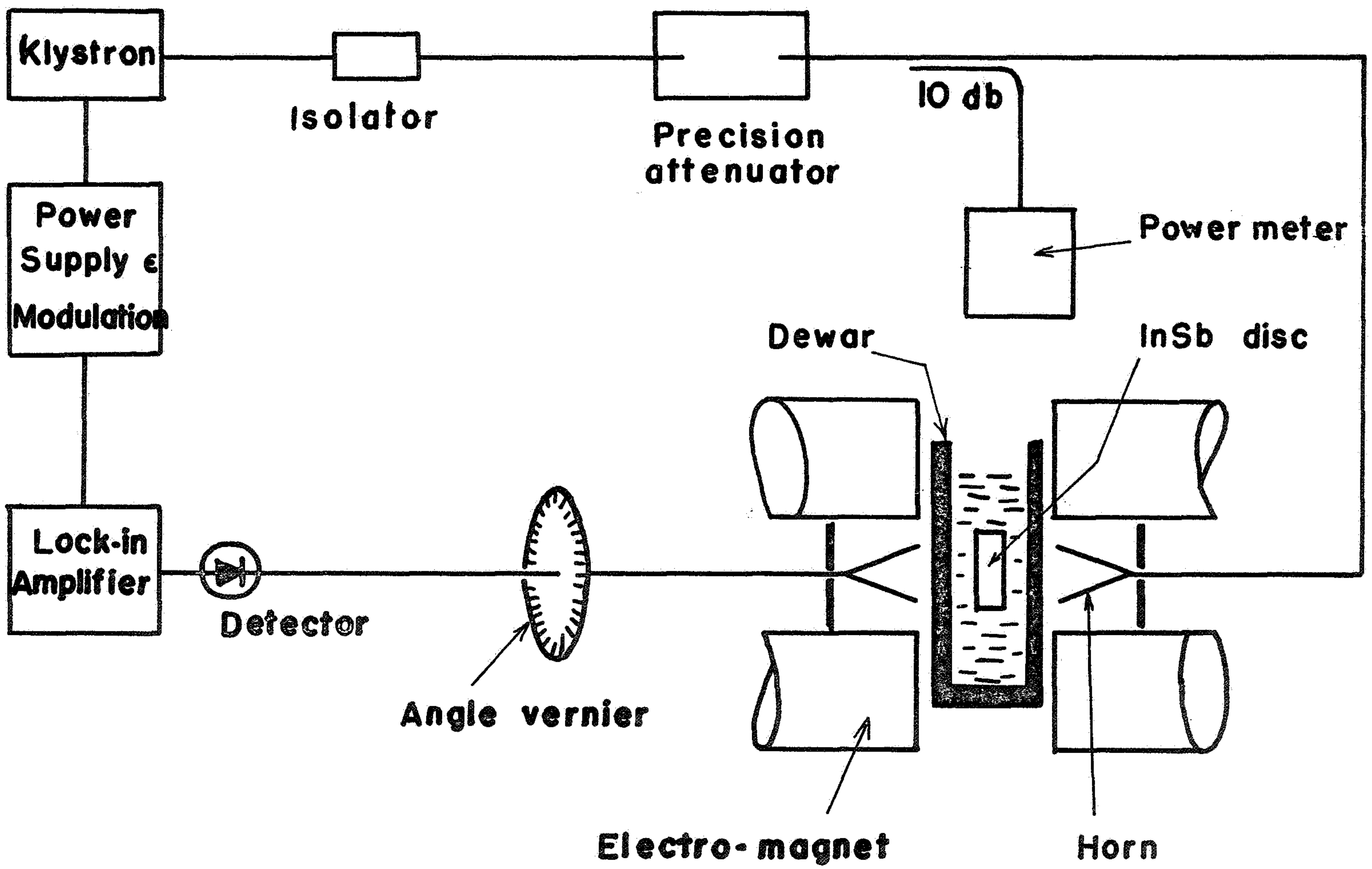

Figure 8 _ Experimental set-up for the Faraday effect measurements

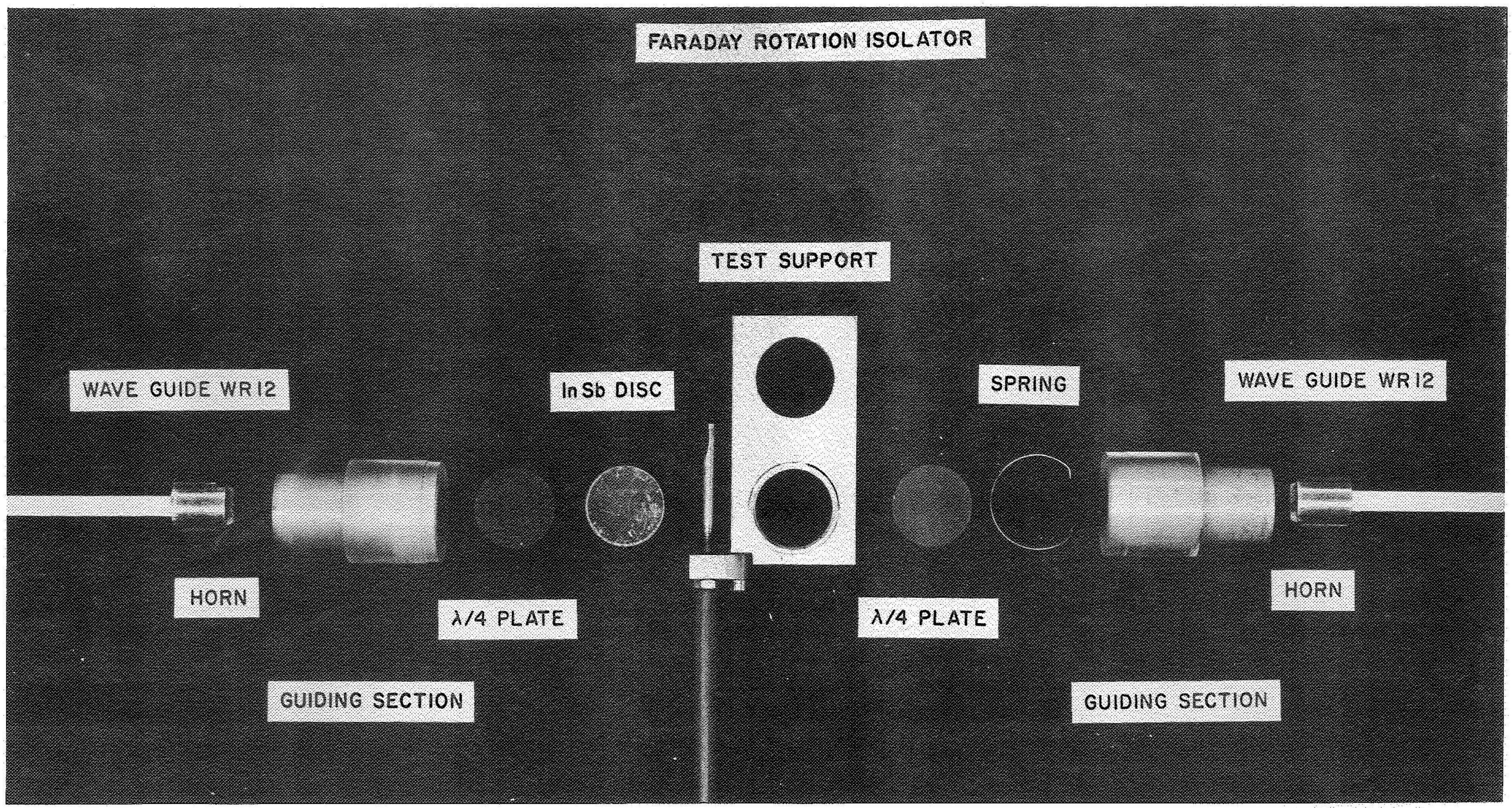

Fig 9 _ Faraday rotation isolator

Table 1: Electrical properties of the n-type InSb crystals.

	Ingot 1 (C2-939)		Ingot 2 (C2-500)
	75°K	300°K	75°K
Energy gap (eV)	0.26	0.16	0.26
Carrier density (cm^{-3})			
- electrons	2.8×10^{14}	1.3×10^{16}	3.5×10^{13}
- holes	$\sim 1.7 \times 10^{5}$	1.3×10^{16}	
Effective mass			
- electrons	$0.013 m_o$	$0.013 m_o$	$0.013 m_o$
- holes	$0.6 m_o$	$0.6 m_o$	$0.6 m_o$
Mobility ($cm^2 V^{-1} s^{-1}$)			
- electrons	530.000	~50000	340000
- holes	~10000	~750	~10000

readily measured. The coupling between the two horns when the wave propagates through the semiconductor plasma is maximum in Fig. 10a and minimum in Fig. 10b, zero if the transmitted wave is linearly polarized as when there is no sample in the wave path. The ratio of the minimum to the maximum coupling gives the ellipticity of the polarization.

At room temperature with the crystal in place no wave was detected. At 75°K with no magnetic field, no transmission was detected. With an increasing magnetic field applied to the sample, transmission also increased and reached a limiting value at high magnetic field. With the field applied in either direca_ Maximum coupling

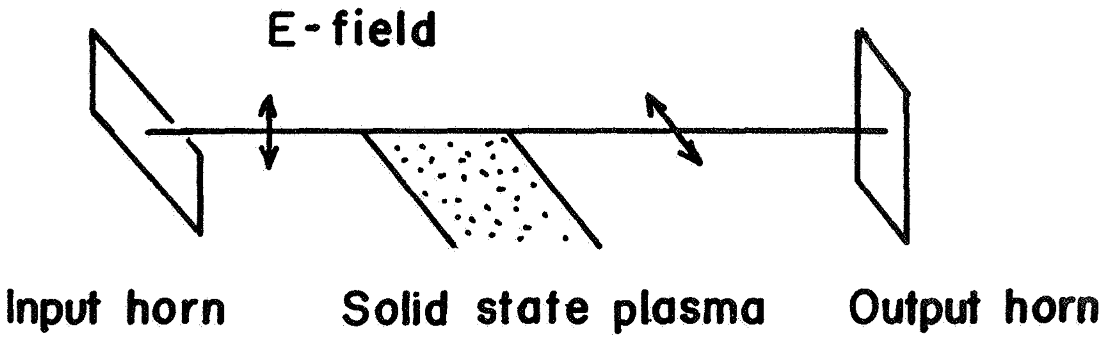

b_ Minimum coupling

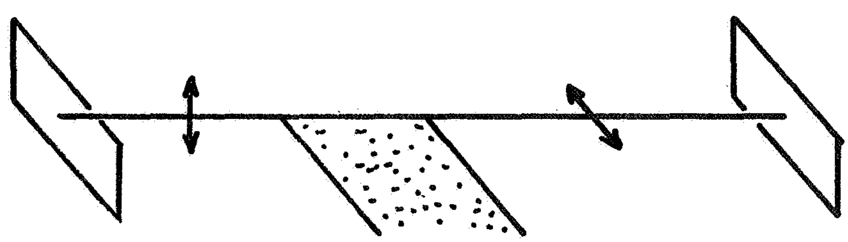

Figure 10_ Orientations of the horns for maximum and minimum couplings

tion the effect was seen to be the same but the direction of the polarization was changed.

The measurements of Faraday rotation and loss where performed on two discs of InSb as a function of magnetic field, the results are shown in Figures 11 and 12.

In order to minimize the losses inherent to reflections from the flat surfaces of the sample, quarter wave impedance transformers were placed on both sides of the sample. The use of quarter wave matching plates works well in this case since the dielectric constants of the semiconductor for the two polarizations do not differ greatly. The dielectric material used had a relative dielectric constant of about 4. With this configuration measurements of Faraday rotation and loss were repeated. The results are plotted in Figures 11 and 12. The comparison of the theoretical prediction and the experimental results show a good agreement.

2.4 Non-Reciprocal Quasi-Optical Devices

We have shown that large Faraday rotation angles per unit length can be achieved with little loss in a solid state plasma in strong magnetic fields. The device so obtained can be called a rotator and will be the basic element for the devices described in this section.

The nonreciprocity of the Faraday effect was demonstrated when the magnetic field was reversed. This nonreciprocity in effect, can also be termed as: the plane of polarization of the

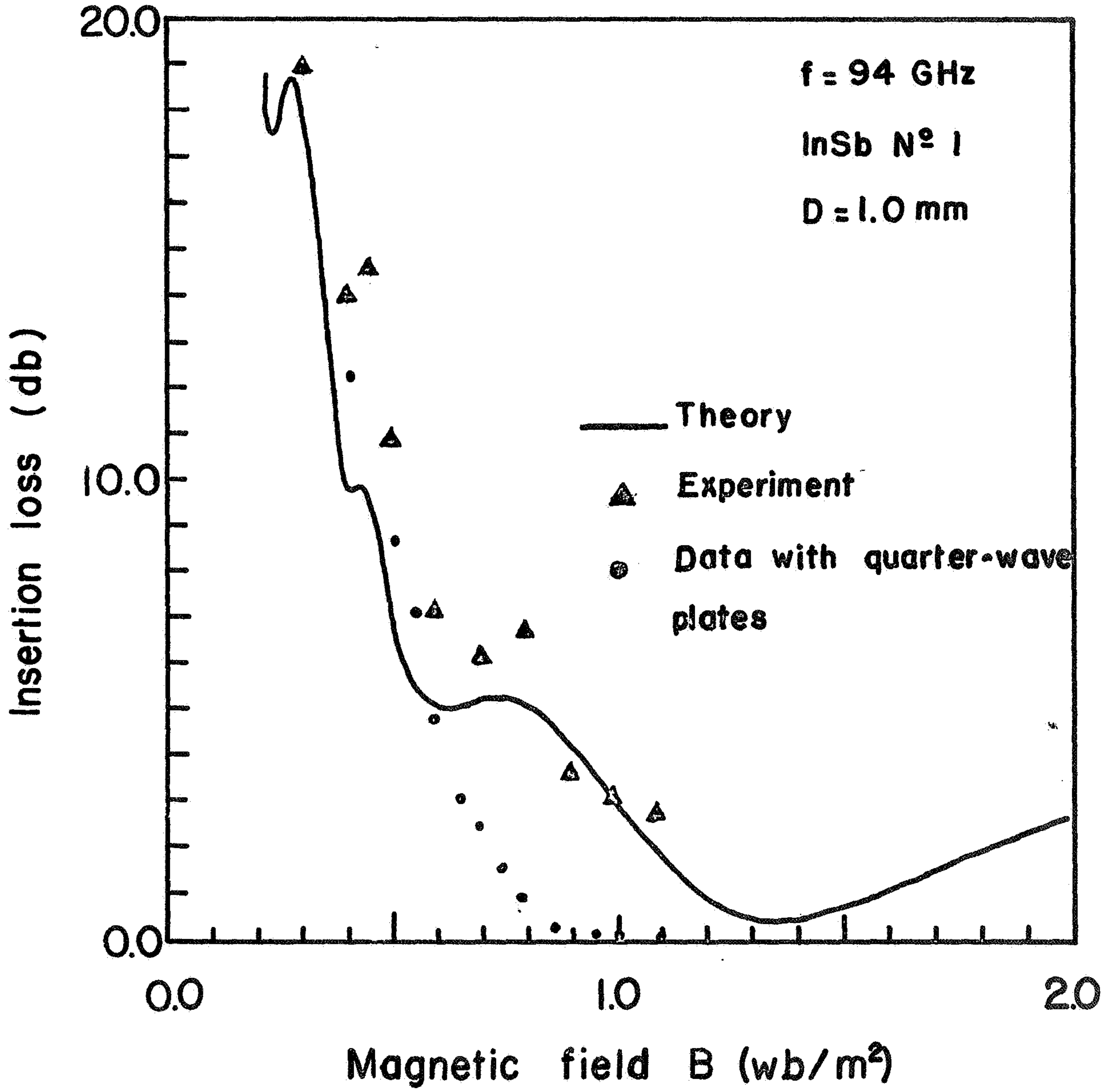

Figure 11 _ Comparison of theory and experimental data

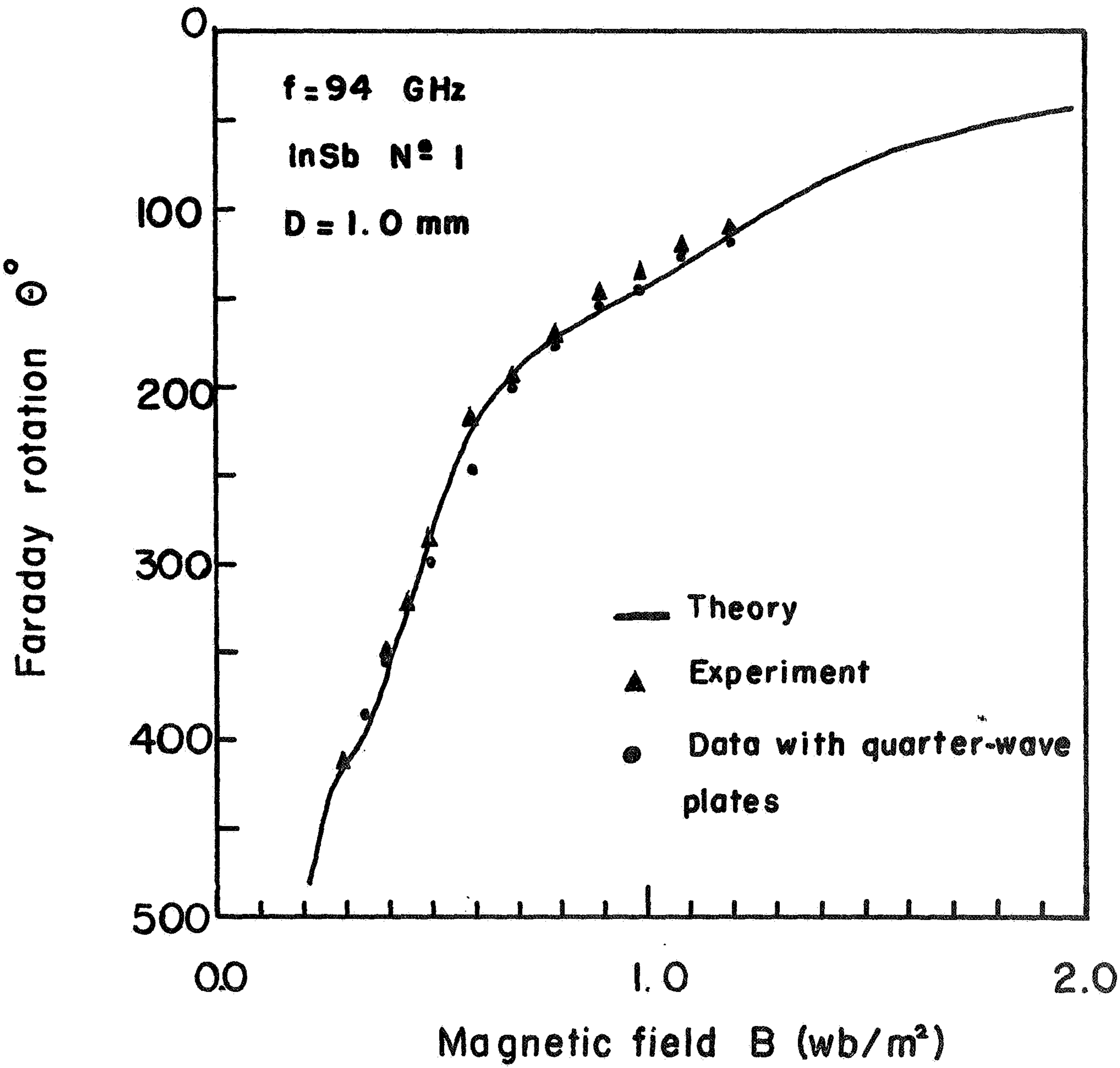

Figure 12 _ Comparison of theory and experimental data reflected wave does not return to the position it had with the incident wave. Therefore, referred to the plane of polarization of the incident wave, the reflected wave plane of polarization is seen to have suffered a rotation angle equal to twice the Faraday rotation for a single pass.

The experiments were designed to test an isolator and a three port circulator using InSb at 75°K. For these devices, the rotation for a single pass through the sample was set at 135° so that the assumptions for large magnetic fields:

$$\omega_c \tau >> 1 \qquad\qquad \omega_c > \omega$$

held. In this high field range the loss through the sample is seen to be less than 1 db with the configuration using the quarter wave plates. It should be noted that these will be necessary in the designing of any practical device.

2.4.1 Isolators

The design of the isolator at 94 GHz used basically the same components as the one shown in Fig. 9. The isolating structure sketched in Fig. 13 is made of mica fins covered with resistive paint and imbedded in a styrofoam support. An insertion loss of 30 db was measured in a free space setup, i.e., placed in between two high gain horns. The wave traveling from the source, left to right, experiences a 135° clockwise rotation through the solid state plasma rotator. The receiving horn is rotated 135° so that the wave is transmitted in the output waveguide. The reflected wave propagating in the reverse

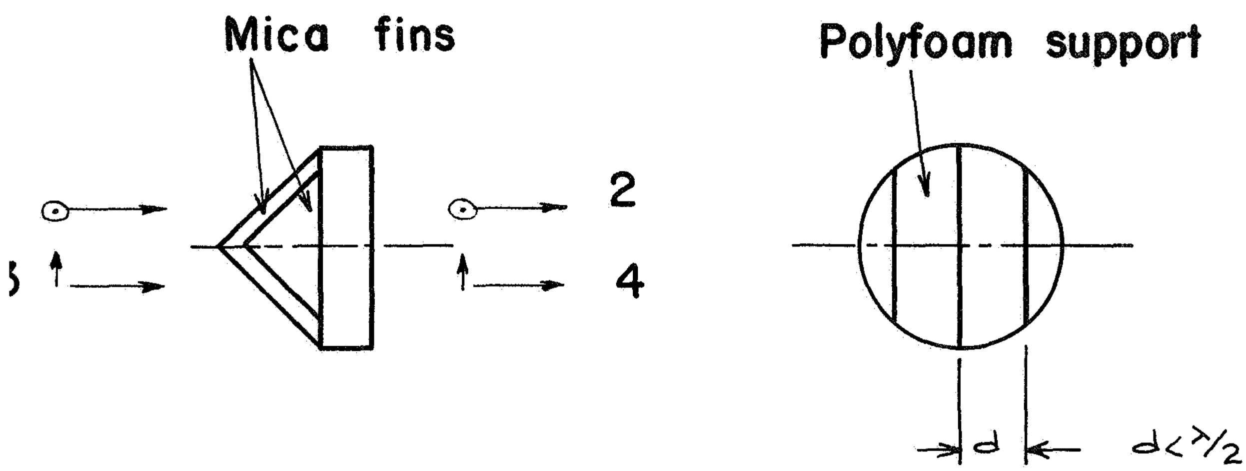

1 → 2	< 1db
3 → 4	~ 30db

Figure 13 — Isolator structure

direction will go through the solid state plasma again where it will suffer a 135° rotation counterclockwise this time. So the electric field is oriented at 270° from its original position. It is then parallel to the fins of the isolating structure, consequently the reflected wave will be absorbed. The losses suffered by the wave going from one horn to the other in the absence of the isolating structure has been measured to be 13 db. This large value is due to poor horn design and could be reduced with more care given to the design of the waveguide to free-space transition. The forward loss due to the isolating structure, which was theoretically and experimentally less than 1 db, could not be measured because it was so small.

The best difference between forward and reverse attenuation of the solid state plasma isolator was only 9 db. It is believed that this low isolation is due to the reflections in the quasi-optical structure designed, notably for example, at the low gain horns.

2.4.2 Circulator

The circulator design uses components similar to the ones shown in Fig. 9. The circulator structure drawn in Fig. 14 was placed into the test supporter. Its characteristics in the absence of the solid state plasma are given also in Fig. 14. The forward loss of about 1 db when the electric vector is perpendicular to the fins. The insertion loss obtained when the

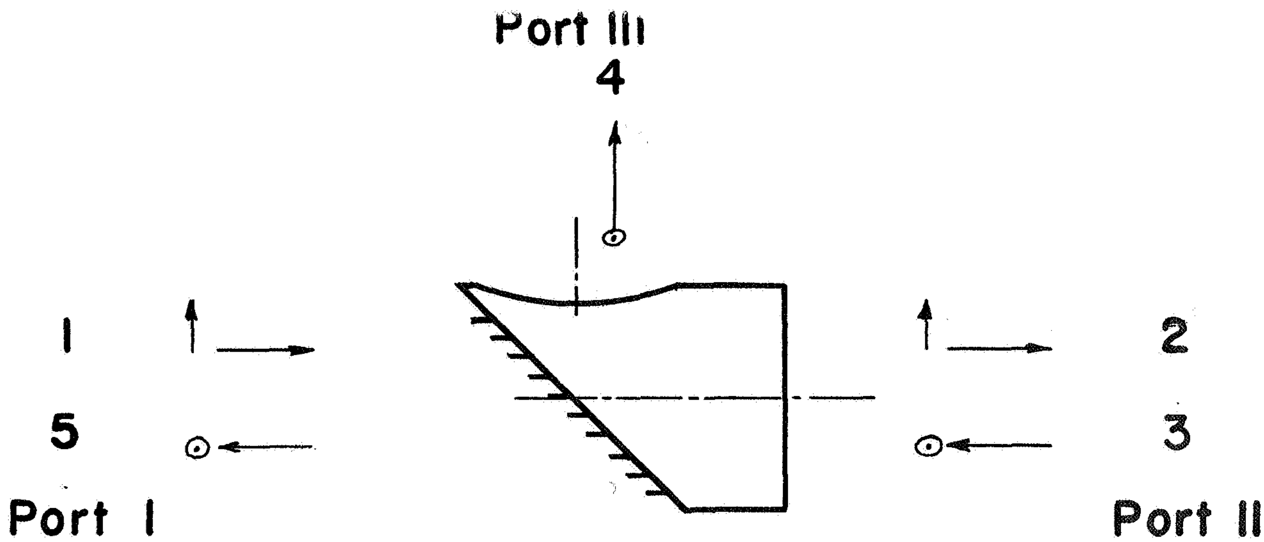

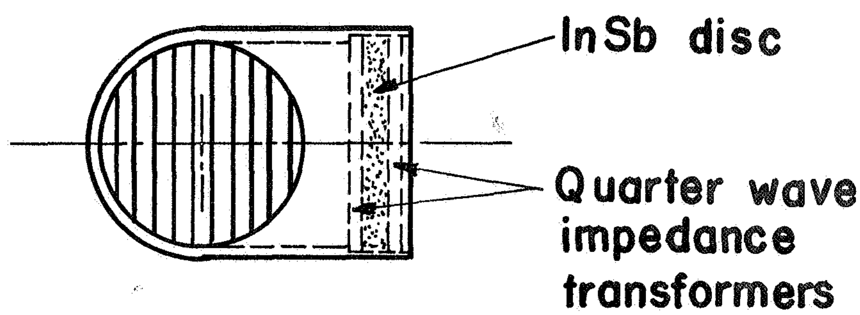

1 → 2	~ 1 db
3 → 4	~ 2.5db
3 → 5	~ 40db
4 → 5	> 40 db*

INPUT		OUTPUT		
		Port I	Port II	Port III
Port I	⊙	0	~40 db	High *
	↑	0	~ 1 db	High *
Port II	⊙	~40db	0 db	~2.5 db
	↑	~ 1 db	0 db	High *
Port III	⊙	High *	~2.5 db	0
	↑	High *	High *	0

*Not measured but >40 db

Figure 14 _ Circulator structure

electric vector is parallel to the fins was over 40 dbs. The coupling from port II to port III showed a loss of about 2.5 db.

The expected circulator performance is presented in Fig. 14. The feasibility of this service also depends very much on the design of the quasi-optical section as does the isolator. However, with sufficient care, low loss quasi-optical guiding systems can be designed.

2.5 Conclusions

The experimental investigation of the microwave Faraday effect in a solid state plasma under a large magnetic field and the theoretical results predicted by Donovan and Medcalf theory have been compared. The results show that they are in good agreement for magnetic fields up to 1.3 Wb/m^2 and with n-type indium antimonide at liquid nitrogen temperature.

We have found that a large rotation of the plane of polarization of the quasi-optical incident electromagnetic wave can be obtained with little loss. This property led to the study of various microwave devices using the Faraday effect.

We have seen that mm wavelength Faraday rotators utilizing InSb at cyrogenic temperature required magnetic fields of only a few kilogauss to be feasible. Isolators having a forward loss of about 1 db and an isolation of 9 db were built using Faraday rotation.

In the investigation of quasi-optical isolators and circulators we have concluded that care must be taken in designing any waveguide to free space transitions, although this would be an insignificant problem in totally quasi-optical system since the feasibility of the described devices is very dependent upon lowering of the losses inherent to their designs.

In the three cases investigated we have found that for a low loss solid state plasma the following inequality must be satisfied $\mu\beta >> 1$. With indium antimonide this condition was easily reached at liquid nitrogen and with moderately high magnetic fields. However, these two physical requirements may limit the practicality of such devices to specialized systems. It is not anticipated that this situation could change with the improvement of the known semiconductors. Indium arsenide was considered to be a possibility for room temperature operation, but its intrinsic concentration is high enough to result in the requirement of a magnetic field of about 10 Wb/m^2 in order to satisfy the low loss condition mentioned before.

The present work can be extended to the infrared frequency range where the system would then be totally optical. The theory outlined here would be applicable, with a few modifications due to lattice absorption. Devices could be designed for room temperature operation with materials such as indium antimonide and with moderate magnetic fields.

3. WAVEGUIDE ISOLATORS

This work is being performed by M. Kanda and W.G. May.

3.1 Introduction

Nonreciprocal microwave devices such as isolators, circulators, modulators and phase shifters have been considered by using the tensor properties of the permeability [18,19]. Similar nonreciprocal properties have been observed using a gaseous plasma which has a tensor permittivity in a dc magnetic field. [20,21]

Recently solid-state plasmas have been used as the basis of waveguide isolators, using the non-reciprocal tensor properties of the dielectric constant in the presence of a dc magnetic field. In the device reported by M. Toda [22,23] field displacement of the signal propagated through InSb at liquid nitrogen temperature in the presence of a transverse dc magnetic field was used to achieve isolation. Another isolator was developed using Faraday rotation in a waveguide filled with InSb under a longitudinal magnetic field. [6,7,24,25]

In this report, the microwave propagation characteristics of a waveguide isolator using an InSb rod and an InSb annulus at 94 GHz and 75°K are presented theoretically and experimentally.

3.2 Waveguide Isolator Employing a Semiconductor Plasma Rod in the Waveguide.

In recent years, wave propagation in waveguides filled or partially filled with a plasma column have been studied. The first extensive study of the configuration of Fig. 15(a) was

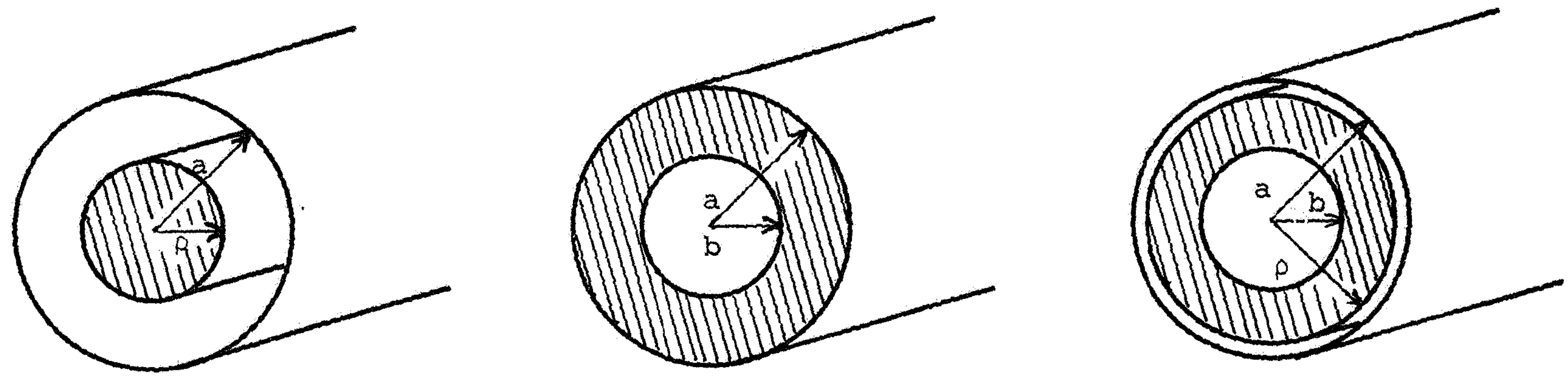

a) InSb Rod-in-Waveguide　　b) Hollow InSb Waveguide　　c) InSb Annulus-in-Waveguide

FIGURE 15. CIRCULAR PLASMA WAVEGUIDE STRUCTURES

done by A.W. Trivelpiece [26], who analyzed propagation characteristics in the presence and absence of an axial dc magnetic field using the quasi-static approximations. Considerable attention has been given to the existence of backward space-charge waves in the plasma. V. L. Granatstein, S. P. Schlesinger, and A. Vigants [27], L. Alfredson [28], R. N. Carlile [29], P. Leprince and J. Pommier [30], and P.J.B. Clarricoats [31] made further studies of the dipolar backward space-charge wave under isotropic plasma conditions.

V. L. Granatstein and S. P. Schlesinger [32], B. Agdur [33], V. Bevc and T. T. Everhart [34], and W. P. Allis, S. J. Buchsbaum and A. Bers [35] have made very detailed studies of a circular waveguide containing an anisotropic plasma rod.

The purpose of this section is to present theoretical and experimental microwave propagation characteristics in a rod of InSb coaxially mounted in the cylindrical waveguide at 94 GHz and 75°K. The inside profile of the complete 94 GHz waveguide isolator partially filled with a rod of InSb is shown in Fig. 16. This isolator is a shorter wavelength version of a device developed previously in this laboratory [10].

The operation of the isolator depends on the exclusion or absorption of a circularly polarized 94 GHz microwave signal by a rod of InSb, coaxially mounted in a cylindrical waveguide. The extent of the exclusion or absorption depends on the sense of the microwave signal polarization and the applied axial dc magnetic field.

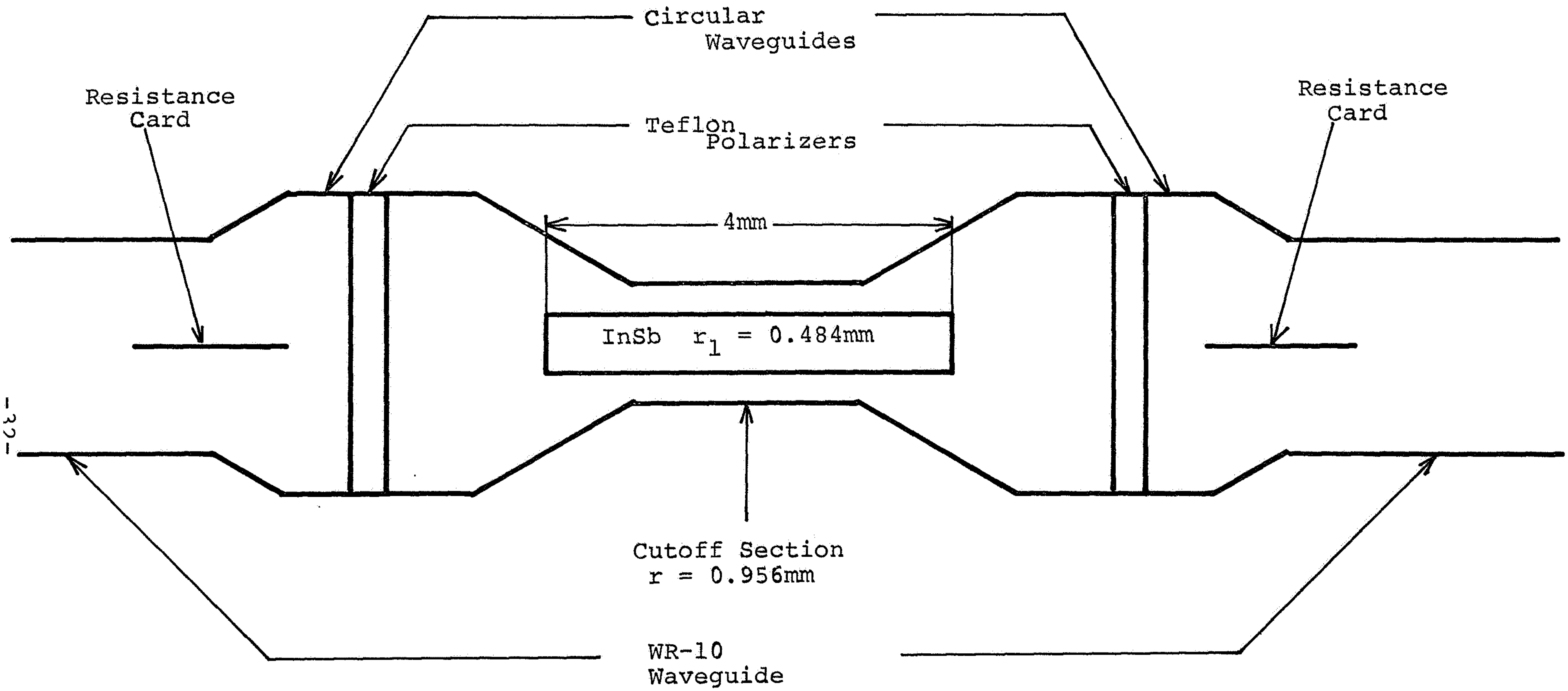

FIGURE 16. INSIDE PROFILE OF THE 94 GHZ InSb ROD-IN-WAVEGUIDE ISOLATOR

3.2.1 Theoretical Calculations

With a longitudinal dc magnetic field in the InSb rod, the total dielectric constant of the material, due to both lattice and carriers, seen by the microwave signal depends on the direction of circular polarization with respect to the magnetic field. The total relative dielectric constant is expressed as

$$\varepsilon_{\pm} = \varepsilon' + j\varepsilon'' \tag{3.1}$$

where

$$\varepsilon'_{\pm} = \varepsilon_{\ell}\left(1 - \frac{\omega_p^2 \tau^2 (\omega_{\pm}\omega_c)}{\omega[1 + \tau^2(\omega_{\pm}\omega_c)^2]}\right) \tag{3.2}$$

and

$$\varepsilon''_{\pm} = \varepsilon_{\ell}\left(\frac{-\omega_p^2 \tau}{\omega[1 + \tau^2(\omega_{\pm}\omega_c)^2]}\right) \tag{3.3}$$

The subscripts $\pm$ refer to the right and left hand circular polarized components in the direction of the magnetic field.

For a longitudinal magnetic field B_o large enough that $\omega_c \gg \omega, \tau^{-1}$ these above expressions are

$$\varepsilon'_{\pm} \cong \varepsilon_{\ell}\left(1 \mp \frac{\omega_p^2}{\omega\omega_c}\right) = \varepsilon_{\ell}\left(1 \mp \frac{ne}{\omega\varepsilon_{\ell} B_o}\right) \tag{3.4}$$

and

$$\varepsilon''_{\pm} \cong \varepsilon_{\ell}\left(- \frac{\omega_p^2}{\omega\omega_c^2 \tau}\right) = - \frac{nm^*}{\omega\tau B_o^2} \quad . \tag{3.5}$$

It is readily seen that the dielectric constant could be relatively large for a microwave signal circularly polarized one way but very low or even negative for the opposite circular polarization. Let us consider the device shown in Fig. 16, which consists of a cylindrical waveguide surrounding a rod of InSb. If the dc magnetic field is adjusted so that ε'_{-} is close to 1, the waveguide appears empty (aside from loss) to a signal circularly polarized in the (-) sense. This (-) mode strongly excites fields in the InSb, and because of the lossy part of the dielectric constant ε''_{-}, much of the signal rotating in the (-) mode will be absorbed by the InSb. However, the same signal traveling in the opposite direction with respect to B_o, rotates in the (+) sense. Since a signal sees a coaxial structure with the inner conductor being a rod of InSb with $\varepsilon'_{+} = 30$, fields are not excited strongly in the InSb and little power flows in the material. Thus the signal is only very slightly absorbed.

To improve the isolation, the radius r of the circular waveguide containing a rod of InSb is determined in such a way that the empty waveguide is beyond cut-off for the TE_{11} mode in the circular waveguide at the operating frequency, that is [36]

$$r < \frac{1.841c}{\omega} = \frac{1.841\lambda o}{2\pi} \tag{3.6}$$

But r is large enough that a coaxial structure with a center conductor of radius r_1 will propagate a TE_{11} coaxial mode, requiring [36]

$$\frac{r+r_1}{2} > \frac{c}{\omega} = \frac{\lambda o}{2\pi} \quad (3.7)$$

The (+) mode now propagates by exciting the TE_{11} coaxial mode but the (-) mode cannot propagate when $\varepsilon' \sim 1$ because, in the lossless case, the signal sees a waveguide beyond cut-off, and with loss, the fields strongly excited in the InSb are absorbed. In the latter case, the fields are concentrated more in the rod of InSb than they are when the waveguide is not cut off, and the loss is insignificant.

The exact solution for longitudinally magnetized cylindrical waveguide partially filled with a lossless tensor dielectric medium shown in Fig. 15(a) has been done by A. Bers [35]. This solution has been extended to include loss, and with the aid of the digital computer, the solution for the complex propagation constant has been obtained. From these results the attenuation as a function of dc magnetic field can be obtained for two modes and is shown in Fig. 17. It should be noted that this attenuation is for a unit length of waveguide and does not account for any reflection on coupling to different modes that occurs at the ends of the semiconductor-loaded waveguide section.

3.2.2 Experimental Results

The material chosen for the plasma rod is n-type InSb since the free carriers of this material have a high mobility at 75°K. By means of Van der Pauw's technique [17], the free car-

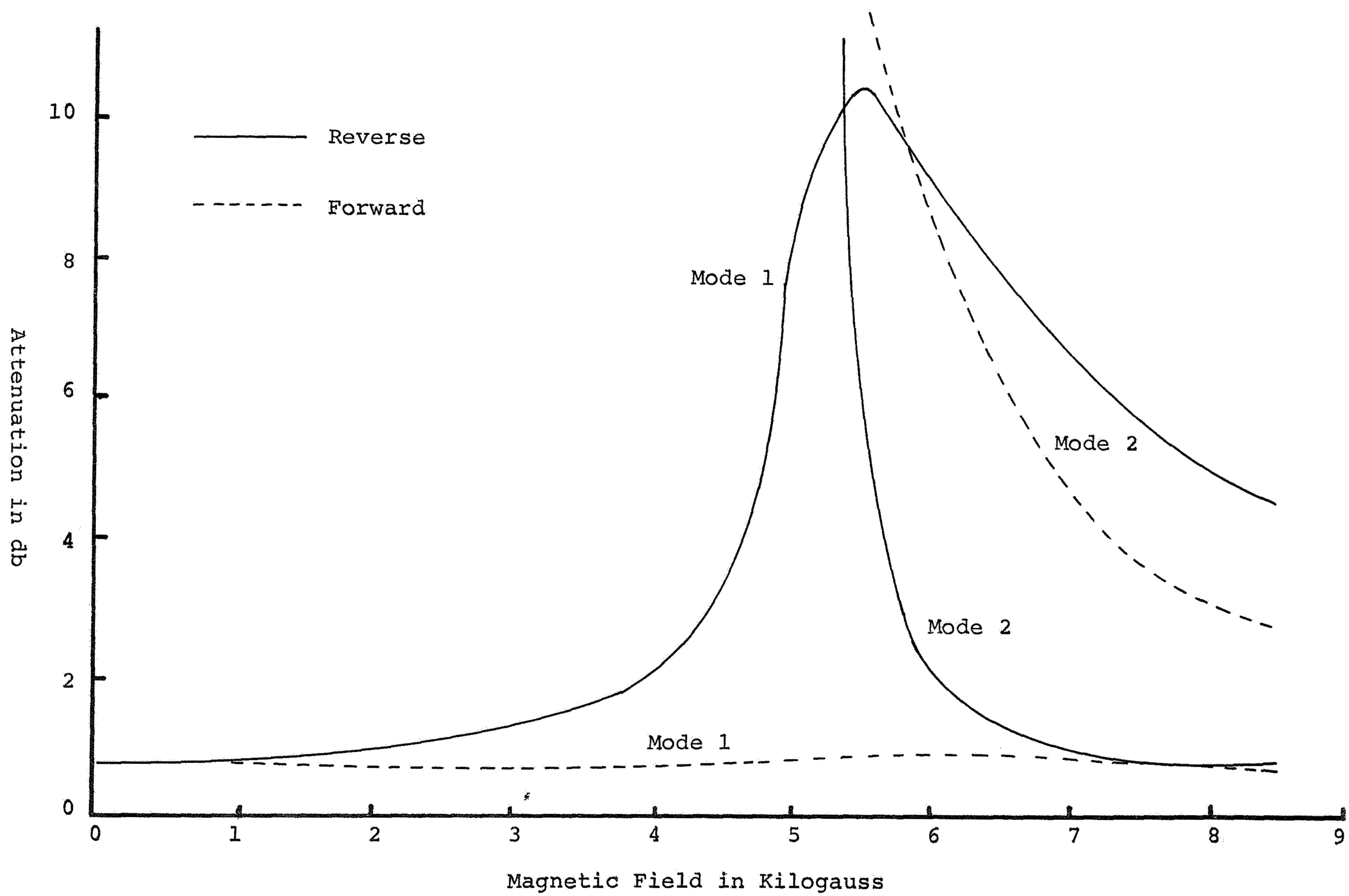

FIGURE 17. CALCULATED ATTENUATION FOR InSb ROD-IN-WAVEGUIDE ISOLATOR

rier concentration of the n-type InSb at 75°K was measured to be

$$n = 2.80 \times 10^{14} \text{ carriers/cc}$$

and the mobility at 75°K is

$$\mu = 5.2 \times 10^{5} \text{ cm}^2\text{/volt-sec.} \ .$$

The device sketched in Fig. 16 consists of rectangular to circular transitions with resistance cards, teflon quarter-wave plates converting the linearly polarized TE_{11} mode to the circularly polarized TE_{11} mode, and a rod of n-type InSb coaxial with the circular waveguide supported and fully surrounded by styrofoam inserts. This device is placed in a longitudinal magnetic field using 6-inch Varian magnet with a 2-inch gap. A styrofoam Dewar surrounds the circular waveguide containing the InSb bar, and this section is filled with liquid nitrogen. The attenuation data as a function of the magnetic field taken for the applied magnetic field parallel and anti-parallel to the direction of microwave propagation, are shown in Fig. 18.

3.2.3 Discussion

The maximum reverse attenuation 24.5 db is obtained at the dc magnetic field 5.3 kG, the value for which ε'_- becomes small as predicted from (3.4). The minimum forward loss is about 3 db excluding the 5 db loss due to polarizers, transitions and waveguide away from the InSb, and no attempt was made to match the semiconductor structure to the remaining waveguide.

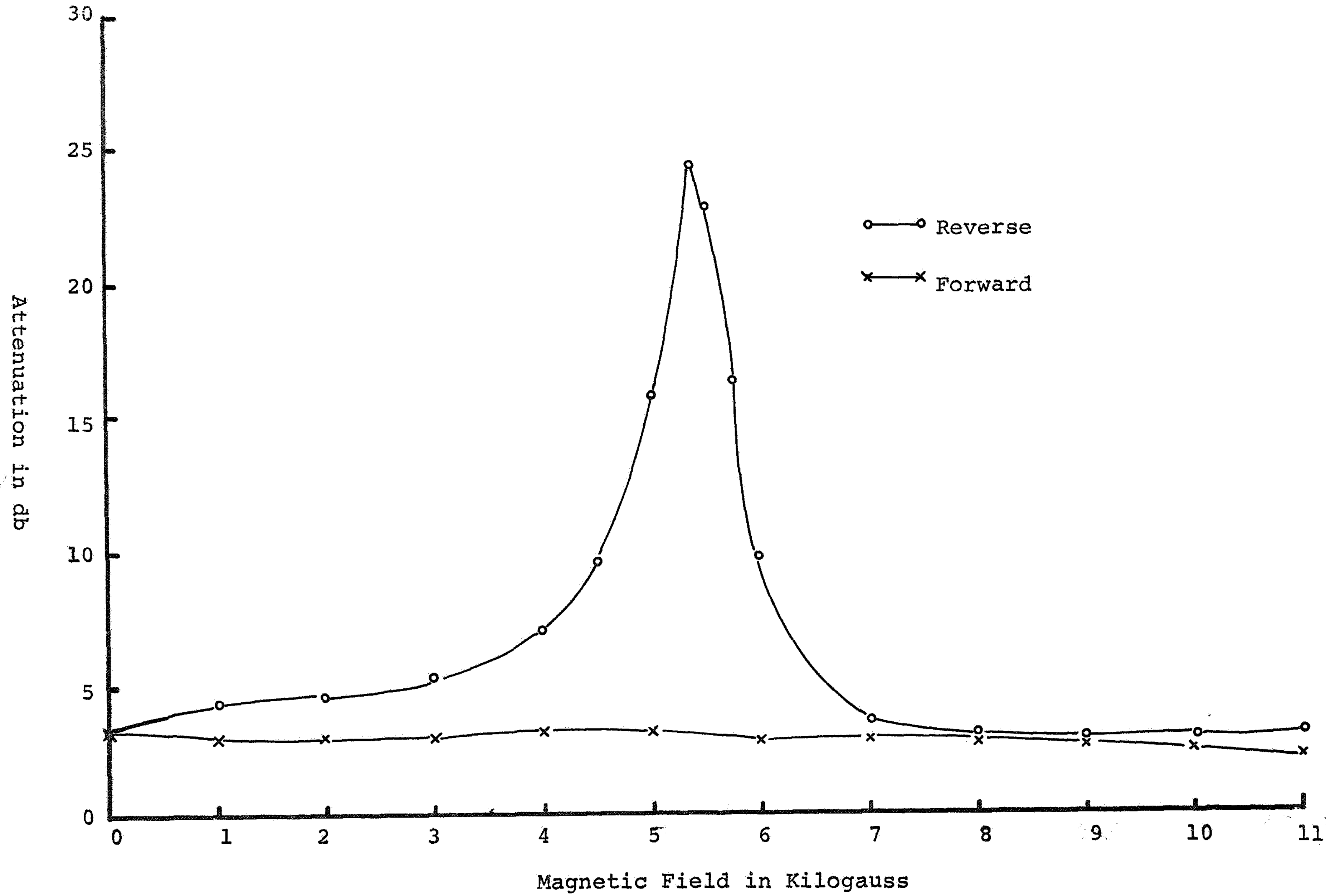

FIGURE 18. EXPERIMENTAL RESULTS FOR InSb ROD-IN-WAVEGUIDE ISOLATOR

The attenuation curves obtained experimentally for the 94 GHz isolator using a rod of InSb do not agree well with the theoretical ones, but this experimental curve could be explained as the mode mixing on the basis of calculated field patterns [10]. That is, the two modes shown in Fig. 17 may be both excited by the TE_{11} mode in the unloaded waveguide, the relative excitation of the two modes being dependent on the magnitude and the direction of the magnetic field. This mode mixing does not take place for the circular waveguide containing a rod of InSb with lower carrier density ($n \cong 4 \times 10^{13}$) [10].

3.3 Waveguide Isolator Employing A Semiconductor Annulus

The waveguide properties of the annular-shaped plasma column shown in Fig. 15(b) in the absence of the external dc magnetic field were first investigated by S. F. Paik [37]. It is predicted from the theory that such a configuration will support propagation in a backward wave mode. These backward waves were observed experimentally by L. S. Napoli and G. A. Swartz [38] using the configuration shown in Fig. 15(c). Exact analysis of the behavior of modes in an annular isotropic plasma column has been made by P. J. B. Clarricoats and J. S. L. Wong [39].

In this section, we present a theoretical analysis of the microwave propagation characteristic of circular waveguides containing an annular anisotropic plasma column shown in Fig.

15(b) and 15(c) and experimental study of the design of a waveguide isolator employing a semiconductor annular plasma column in the waveguide shown in Fig. 19.

Although it is desirable to have simple physical models for the configurations shown in Fig. 15(b) and 15(c) to estimate performance for the isolator, this has not been done because of complexity of the geometry.

3.3.1 Theory

The exact solution to the boundary value problem resulting when the cylindrical waveguide contains a hollow plasma column shown in Fig. 15(b) can be done and is outlined in Appendix A. We assume that the plasma is homogeneous and anisotropic, and that the fields have a z dependence of the form exp $(-\Gamma z)$ where Γ, the propagation constant, is independent of the position z. The characteristic equation is found to be 6x6 determinant given in (A-19). This formidable computational problem can only be done with the aid of the digital computer. This theory does not account for reflection or coupling at the ends of the plasma column.

Also the microwave propagation characteristic for the coaxial waveguide containing the annular InSb plasma shown in Fig. 15(c) is outlined in Appendix B. In order to solve for the appropriate propagation constant, it is required to solve an 8x8 determinant given in (B-11).

3.3.2 Experimental Results

The n-type InSb chosen for the plasma medium has the same

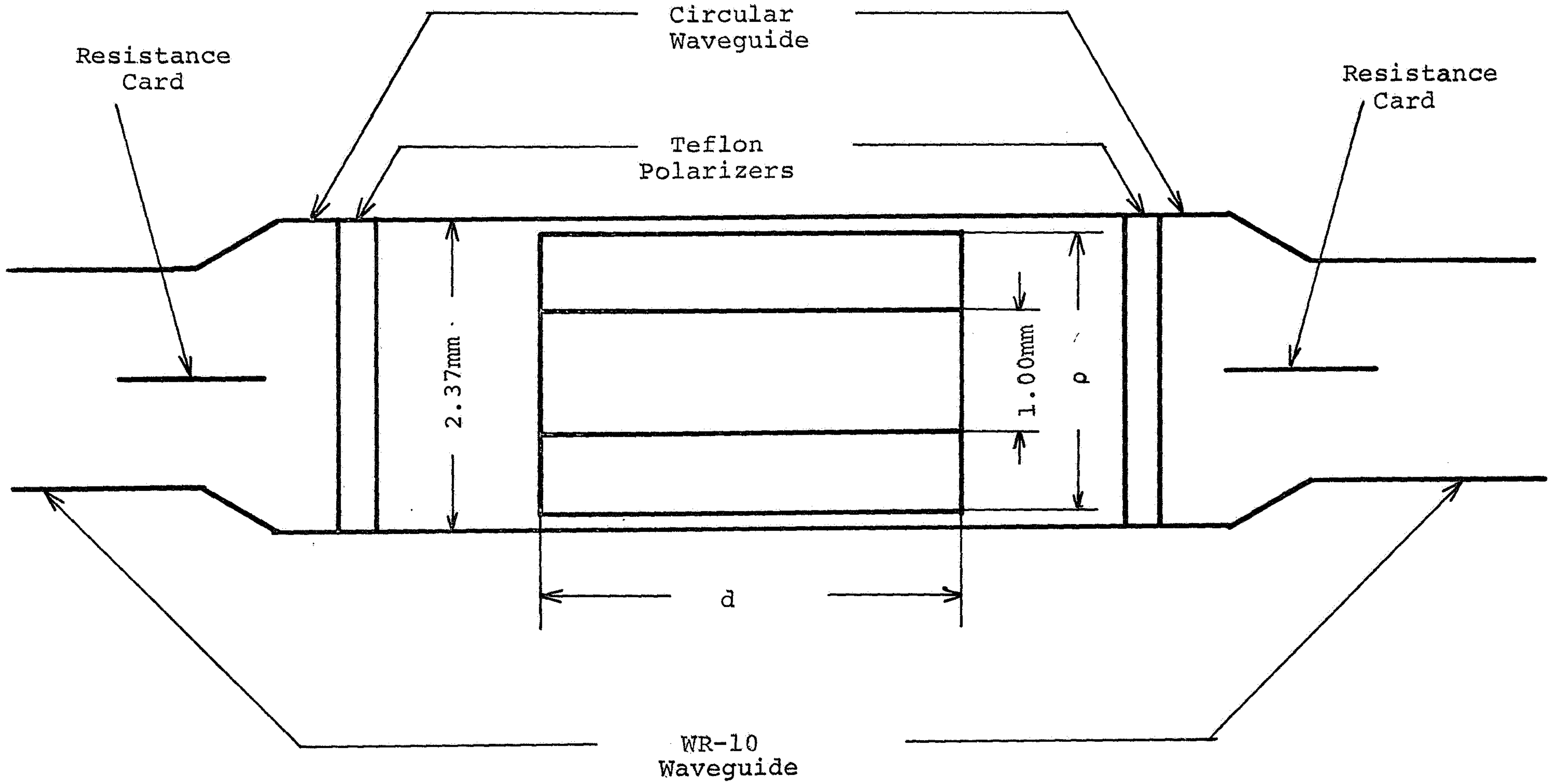

FIGURE 19. INSIDE PROFILE OF THE 94 GHZ InSb ANNULUS-IN-WAVEGUIDE ISOLATOR

electrical characteristics as in the experiment in section 3.2. The annular InSb columns were cut by using an ultra-sonic drill and were polished chemically in a bromine and methanol etch. The device shown in Fig. 19 is essentially the same as in the experiment in section 3.2 except for the central test section. The annular InSb column was supported by styrofoam in this section. The small opening between annular InSb column and circular waveguide wall was filled by using silver paint. The experimentally determined attenuation for the two directions of propagation along the magnetic field are shown in Fig. 20.

Also the coaxial waveguide containing the annular InSb plasma shown in Fig. 15(c) was investigated. Using this device, the experimentally determined attenuation for two directions of propagation along the magnetic field are shown in Fig. 21.

3.3.3 Discussion

The measure of isolation, 20 db with forward loss 2.5 db or 29 db isolation with a forward loss of 6 db was obtained using the annular plasma column waveguide shown in Fig. 15(c). An isolation of 24 db with forward loss of 7 db was obtained using the hallow plasma waveguide shown in Fig. 15(b). The forward losses indicated here are the insertion losses which occur in the test section only and do not include the loss due to polarizers, transitions and waveguide away from the test section. The thinner (0.5 to 1 mm) annular InSb columns give lower insertion.

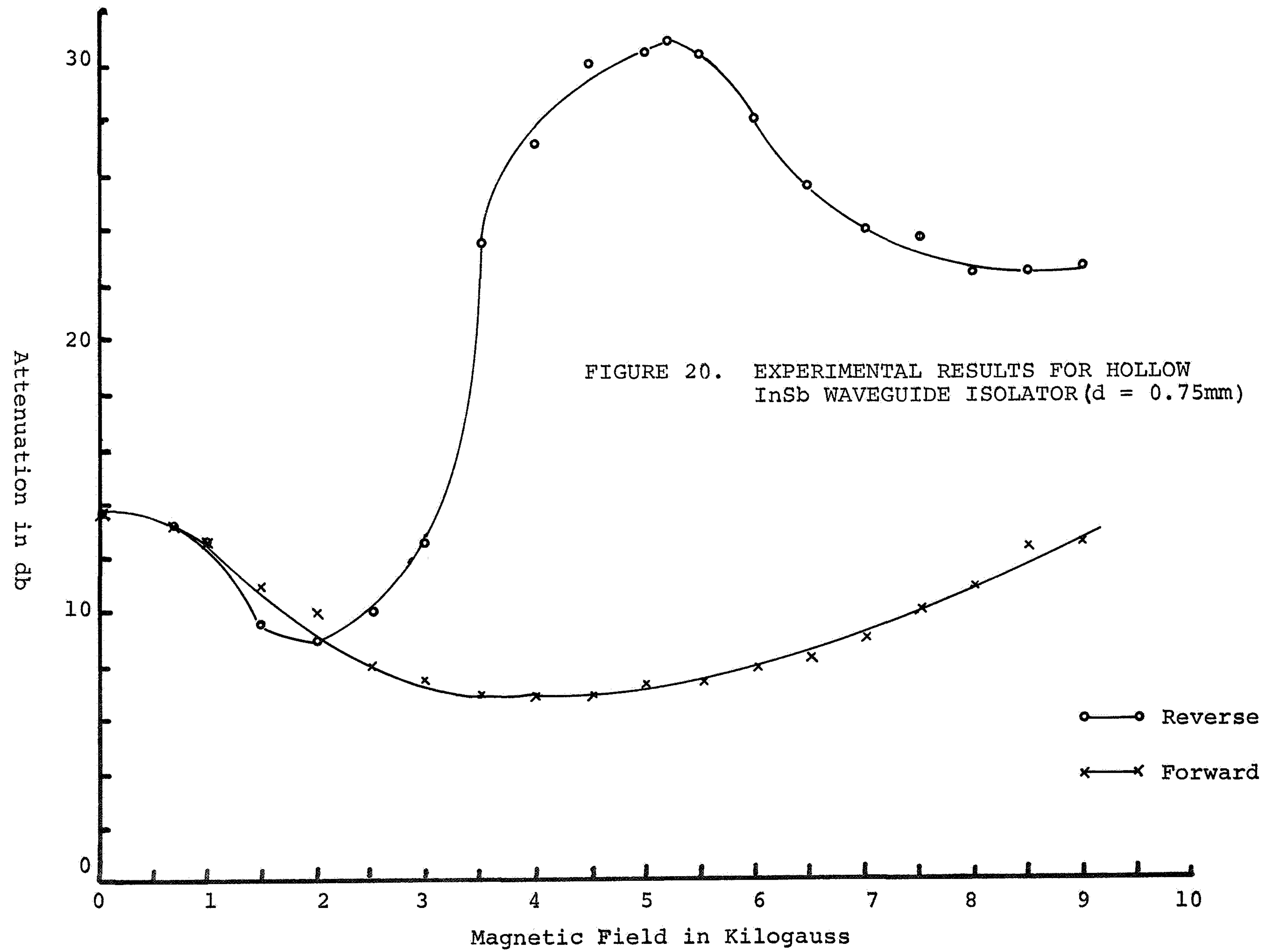

FIGURE 20. EXPERIMENTAL RESULTS FOR HOLLOW InSb WAVEGUIDE ISOLATOR (d = 0.75mm)

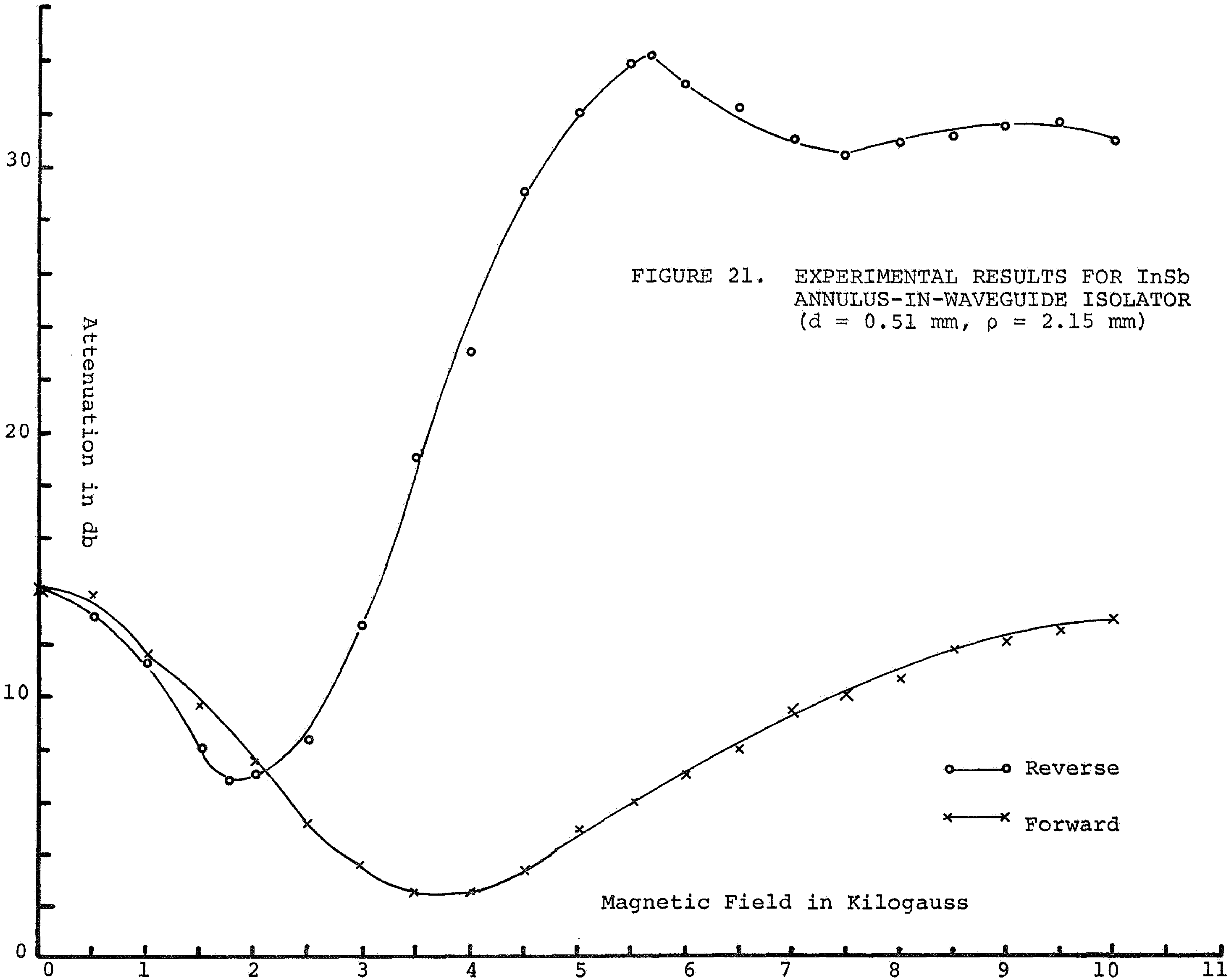

FIGURE 21. EXPERIMENTAL RESULTS FOR InSb ANNULUS-IN-WAVEGUIDE ISOLATOR ($d = 0.51$ mm, $\rho = 2.15$ mm)

Since the length of the annular InSb column is much smaller than the wavelength, end effects should be taken into account. However, this is a quite formidable problem and has not yet been tackled successfully.

3.4 Conclusion

The experiment demonstrated that 20 to 30 db of isolation could be achieved by using three different types of solid-state plasma waveguide isolators shown in Fig. 15 with insertion loss ~2.5 to 5 db. However, the insertion loss could be reduced by very careful design and construction of the isolator.

It will be of interest to extend the preceding investigations to much higher frequency such as infra-red region, since stable and powerful lasers are available nowadays for communication purposes.

4. DISCUSSION AND FUTURE PLANS

The results that are presented in this report demonstrate that it is feasible to develop isolators that are either of the quasi-optical type or of the waveguide type by taking advantage of the anisotropic dielectric constant for a semiconductor plasma in a magnetic field. In all of the cases considered, the forward loss of the isolator could be made small only by cooling the semiconductor. This is necessary to achieve long collision times and to reduce the carrier density in a material such as InSb so that the operating frequency is above the electron plasma frequency. For this reason, it is not felt that the semiconductor plasma devices will be competitive with ferrite devices except in those systems in which cooling is already present, such as in maser systems. In fact, a quasi-optical InSb isolator is being considered for use in a millimeter wavelength maser being constructed at the University of Colorado.

At higher frequencies, in the far infrared portion of the spectrum, nonreciprocal semiconductor devices can be operated at room temperature, and thus are reasonable candidates for a wide range of applications. For example, a Faraday rotation device has been operated at 10.6 microns. The development of coherent sources in the submillimeter portion of the spectrum has made the need for radiation control components very pressing. Thus, the future efforts supported by this grant will be aimed at developing prototype devices operating in the 10 to 1000 micron range, with particular emphasis on isolators. These will be of the Faraday rotation type and also of the reflected beam.

APPENDIX A. CHARACTERISTIC EQUATION FOR HOLLOW InSb WAVEGUIDE

Appendix A gives outlines of the boundary value problem that results from the configuration shown in Fig. 15(b).

The longitudinal field components for r<b are

$$E_z^o = UJ_m(qr)e^{jm\phi-\Gamma z} \tag{A.1}$$

and

$$H_z^o = VJ_m(qr)e^{jm\phi-\Gamma z} \tag{A.2}$$

where U and V are arbitrary, complex constants. The transverse E field components for r<b are

$$E_r^o = \left(Uq\xi J_m'(qr) - Vj\zeta\frac{Z_o m}{qr} J_m(qr)\right)e^{jm\phi-\Gamma z} \tag{A.3}$$

and

$$E_\phi^o = \left(U\frac{jm}{r}\xi J_m(qr) + V\zeta Z_o J_m'(qr)\right)e^{jm\phi-\Gamma z} \tag{A.4}$$

Also the transverse H field components for r<b are

$$H_r^o = \left(Uj\zeta\frac{Y_o m}{qr} J_m(qr) + Vq\xi J_m'(qr)\right)e^{jm\phi-\Gamma z} \tag{A.5}$$

and

$$H_\phi^o = \left(-U\zeta Y_o J_m'(qr) + V\frac{jm}{Y}\xi J_m(qr)\right)e^{jm\phi-\Gamma z}. \tag{A.6}$$

The longitudinal field components inside the annular plasma (b<r<a) are

$$E_z = \left(AJ_m(p_1r) + BN_m(p_1r) + CJ_m(p_2r) + DN_m(p_2r)\right)e^{jm\phi-\Gamma z} \tag{A.7}$$

and

$$H_z = \left(Ah_1J_m(p_1r) + Bh_1N_m(p_1r) + Ch_2J_m(p_2r) + Dh_2N_m(p_2r)\right)e^{jm\phi-\Gamma z} \tag{A.8}$$

where A, B, C and D are arbitrary, complex constants.

The transverse E field component inside the annular plasma column $(b<r<a)$ are

$$E_r = \Big[A\Big(-\frac{jm}{r}L_2 J_m(p_1 r) + \ell_2 p_1 J_m'(p_1 r)\Big) + B\Big(-\frac{jm}{r}L_2 N_m(p_1 r) + \ell_2 p_1 N_m'(p_1 r)\Big) + C\Big(-\frac{jm}{r}L_1 J_m(p_2 r) + \ell_1 p_2 J_m'(p_2 r)\Big) + D\Big(-\frac{jm}{r}L_1 N_m(p_2 r) + \ell_1 p_2 N_m'(p_2 r)\Big)\Big] e^{jm\phi - \Gamma z} \tag{A.9}$$

and

$$E_\phi = \Big[A\Big(\frac{jm}{r}\ell_2 J_m(p_1 r) + L_2 p_1 J_m'(p_1 r)\Big) + B\Big(\frac{jm}{r}\ell_2 N_m(p_1 r) + L_2 p_1 N_m'(p_1 r)\Big) + C\Big(\frac{jm}{r}\ell_1 J_m(p_2 r) + L_1 p_2 J_m'(p_2 r)\Big) + D\Big(\frac{jm}{r}\ell_1 N_m(p_2 r) + L_1 p_2 N_m'(p_2 r)\Big)\Big] e^{jm\phi - \Gamma z}. \tag{A.10}$$

For the transverse H field components

$$H_r = \Big[A\Big(-\frac{jm}{r}Y_2 J_m(p_1 r) + y_2 p_1 J_m'(p_1 r)\Big) + B\Big(-\frac{jm}{r}Y_2 N_m(p_1 r) + y_2 p_1 N_m'(p_1 r)\Big) + C\Big(-\frac{jm}{r}Y_1 J_m(p_2 r) + y_1 p_2 J_m'(p_2 r)\Big) + D\Big(-\frac{jm}{r}Y_1 N_m(p_2 r) + y_1 p_2 N_m'(p_2 r)\Big)\Big] e^{jm\phi - \Gamma z} \tag{A.11}$$

and

$$H_\phi = \Big[A\Big(\frac{jm}{r}y_2 J_m(p_1 r) + Y_2 p_1 J_m'(p_1 r)\Big) + B\Big(\frac{jm}{r}y_2 N_m(p_1 r) + Y_2 p_1 N_m'(p_1 r)\Big) + C\Big(\frac{jm}{r}y_1 J_m(p_2 r) + Y_1 p_2 J_m'(p_2 r)\Big) + D\Big(\frac{jm}{r}y_1 N_m(p_2 r) + Y_1 p_2 N_m'(p_2 r)\Big)\Big] e^{jm\phi - \Gamma z}. \tag{A.12}$$

Now the boundary conditions at the plasma surface (r=b) shall be taken as the continuity of the tangential E and H fields.

$$AJ_m(p_1b) + BN_m(p_1b) + (J_m(p_2b) + DN_m(p_2b) = UJ_m(qb) \qquad (A.13)$$

$$Ah_1J_m(p_1b) + Bh_1N_m(p_1b) + Ch_2J_m(p_2b) + Dh_2N_m(p_2h) = VJ_m(qb) \qquad (A.14)$$

$$A\left(\frac{jm}{b}\ell_2J_m(p_1b) + L_2p_1J_m'(p_1h)\right) + B\left(\frac{jm}{b}\ell_2N_m(p_1b) + L_2p_1N_m'(p_1b)\right)$$

$$+ C\left(\frac{jm}{b}\ell_1J_m(p_2b) + L_1p_2J_m'(p_2b)\right) + D\left(\frac{jm}{b}\ell_1N_m(p_2b) + L_1p_2N_m'(p_2b)\right)$$

$$= U\frac{jm}{b}\xi J_m(qb) + V\zeta Z_oJ_m'(qb) \qquad (A.15)$$

$$A\left(\frac{jm}{b}Y_2J_m(p_1b) + Y_2p_1J_m'(p_1b)\right) + B\left(\frac{jm}{b}Y_2N_m(p_1b) + Y_2p_1N_m(p_1b)\right)$$

$$+ C\left(\frac{jm}{b}Y_1J_m(p_2b) + Y_1p_1J_m'(p_2b)\right) + D\left(\frac{jm}{b}Y_1N_m(p_2b) + Y_1p_2N_m'(p_2b)\right)$$

$$= - U\zeta Y_oJ_m'(qb) + V\frac{jm}{b}\xi J_m(qb) \qquad (A.16)$$

Also at the boundary of the perfect conductor waveguide wall (r=a).

$$AJ_m(p_1a) + BN_m(p_1a) + CJ_m(p_2a) + DN_m(p_2a) = 0 \qquad (A.17)$$

$$A\left(\frac{jm}{\rho}\ell_2J_m(p_1a) + L_2P_1J_m'(p_1a)\right) + B\left(\frac{jm}{\rho}\ell_2N_m(p_1a)\right.$$

$$\left.+ L_2P_1N_m'(p_1a)\right) + C\left(\frac{jm}{\rho}\ell_1J_m(p_2a) + L_1P_2J_m'(p_2a)\right)$$

$$+ D\left(\frac{jm}{\rho}\ell_1N_m(p_2a) + L_1P_2N_m'(p_2a)\right) = 0 \qquad (A.18)$$

In order to have non-trivial solutions of A, B, C, D, U and V, the 6x6 determinant of these coefficients must be zero.

$$\begin{vmatrix} J_m(p_1a) & N_m(p_1a) & J_m(p_2a) & N_m(p_2a) & 0 & 0 \\ S_1(p_1a) & S_2(p_1a) & S_3(p_2a) & S_4(p_2a) & 0 & 0 \\ J_m(p_1b) & N_m(p_1b) & J_m(p_2b) & N_m(p_2b) & -J_m(qb) & 0 \\ h_1J_m(p_1b) & h_1N_m(p_1b) & h_2J_m(p_2b) & h_2N_m(p_2b) & 0 & -J_m(qb) \\ S_1(p_1b) & S_2(p_1b) & S_3(p_2b) & S_4(p_2b) & -\frac{jm}{b}\xi J_m(qb) & -\zeta Z_o J_m'(qb) \\ T_1(p_1b) & T_2(p_1b) & T_3(p_2b) & T_4(p_2b) & \zeta Y_o J_m'(qb) & -\frac{jm}{b}\xi J_m(qb) \end{vmatrix} = 0 \qquad \text{(A.19)}$$

APPENDIX B. CHARACTERISTIC EQUATION FOR InSb ANNULUS IN WAVEGUIDE

The derivation of the characteristic equation for the configuration shown in Fig. 15(c) is outlined.

The longitudinal field components for outside the plasma $\rho<r<a$ are

$$E_z^o = WF_{mm}(qr,qa)e^{jm\phi-\Gamma z} \tag{B.1}$$

and

$$H_z^o = XF_{mm'}(qr,qa)e^{jm\phi-\Gamma z} \tag{B.2}$$

where W and X are arbitrary, complex constants.

The transverse E field components for outside the plasma, $\rho<r<a$ are

$$E_r^o = \left[Wq\xi F'_{mm}(qr,qa) - Xj\zeta\frac{Z_o m}{qr}F_{mm'}(qr,qa)\right]e^{jm\phi-\Gamma z} \tag{B.3}$$

and

$$E_\phi^o = \left[W\frac{jm}{r}\xi F_{mm}(qr,qa) + X\zeta Z_o F'_{mm'}(qr,qa)\right]e^{jm\phi-\Gamma z}. \tag{B.4}$$

The transverse H field components are

$$H_r^o = \left[Wj\zeta\frac{Y_o m}{qr}F_{mm}(qr,qa) + Xq\xi F'_{mm'}(qr,qa)\right]e^{jm\phi-\Gamma z} \tag{B.5}$$

and

$$H_\phi^o = \left[-W\zeta Y_o F'_{mm}(qr,qa) + X\frac{jm}{r}\xi F_{mm'}(qr,qa)\right]e^{jm\phi-\Gamma z} \tag{B.6}$$

Using the all field components inside the annular plasma column given in (A.7) to (A.12), let us match the all tangential components of E and H fields at the plasma surface $(r=\rho)$.

$$AJ_m(p_1\rho) + BN_m(p_1\rho) + CJ_m(p_2\rho) + DN_m(p_2\rho) = WF_{mm}(q\rho,qa) \tag{B.7}$$

$$Ah_1J_m(p_1\rho) + Bh_1N_m(p_1\rho) + Ch_2J_m(p_2\rho) + Dh_2N_m(p_2\rho)$$

$$= XF_{mm'}(q\rho, qa) \tag{B.8}$$

Also

$$A\left(\frac{jm}{\rho}\ell_2J_m(p_1\rho) + L_2P_1J_m'(p_1\rho)\right) + B\left(\frac{jm}{\rho}\ell_2N_m(p_1\rho) + L_2P_1N_m'(p_1\rho)\right)$$

$$+ C\left(\frac{jm}{\rho}\ell_1J_m(p_2\rho) + L_1P_2J_m'(p_2\rho)\right) + D\left(\frac{jm}{\rho}\ell_1N_m(p_2\rho) + L_1P_2N_m'(p_2\rho)\right)$$

$$= W\frac{jm}{\rho}\xi F_{mm}(q\rho, qa) + X\zeta Z_oF'_{mm'}(q\rho, qa) \tag{B.9}$$

And

$$A\left(\frac{jm}{\rho}y_2J_m(p_1\rho) + Y_2P_1J_m'(p_1\rho)\right) + B\left(\frac{jm}{\rho}y_2N_m(p_1\rho) + Y_2P_1N_m'(p_1\rho)\right)$$

$$+ C\left(\frac{jm}{\rho}y_1J_m(p_2\rho) + Y_1P_2J_m'(p_2\rho)\right) + D\left(\frac{jm}{\rho}y_1N_m(p_2\rho) + Y_1P_2N_m'(p_2\rho)\right)$$

$$= -W\zeta Y_oF'_{mm}(q\rho, qa) + X\frac{jm}{\rho}\xi F_{mm'}(q\rho, qa) \tag{B.10}$$

Combining the boundary conditions at r=b given in (A.13) to (A.16), one finds the characteristic equation.

$$
\begin{vmatrix}
J_m(p_1b) & N_m(p_1b) & J_m(p_2b) & N_m(p_2b) & -J_m(qb) & 0 & 0 & 0 \\
h_1J_m(p_1b) & h_1N_m(p_1b) & h_2J_m(p_2b) & h_2N_m(p_2b) & 0 & -J_m(qb) & 0 & 0 \\
J_m(p_1\rho) & N_m(p_1\rho) & J_m(p_2\rho) & N_m(p_2\rho) & 0 & 0 & -F_{mm}(q\rho,qa) & 0 \\
h_1J_m(p_1\rho) & h_1N_m(p_1\rho) & h_2J_m(p_2\rho) & h_2N_m(p_2\rho) & 0 & 0 & 0 & -F_{mm'}(q\rho,qa) \\
S_1(p_1b) & S_2(p_1b) & S_3(p_2b) & S_4(p_2b) & -\frac{jm}{b}\xi J_m(qb) & -\zeta Z_o J_m'(qb) & 0 & 0 \\
T_1(p_1b) & T_2(p_1b) & T_3(p_2b) & T_4(p_2b) & \zeta Y_o J_m'(qb) & -\frac{jm}{b}\xi J_m(qb) & 0 & 0 \\
S_1(p_1\rho) & S_2(p_1\rho) & S_3(p_2\rho) & S_4(p_2\rho) & 0 & 0 & -\frac{jm}{\rho}\xi F_{mm}(q\rho,qa) & -\zeta Z_o F_{mm'}'(q\rho,qa) \\
T_1(p_1\rho) & T_2(p_1\rho) & T_3(p_2\rho) & T_4(p_2\rho) & 0 & 0 & \zeta Y_o F_{mm}'(q\rho,qa) & -\frac{jm}{\rho}\xi F_{mm'}(q\rho,qa)
\end{vmatrix} = 0
$$

(B.11)

APPENDIX C. DEFINITION OF TERMS IN APPENDIX A AND B

Definitions of terms used in the solution of the plasma loaded waveguide given in Appendix A and B are listed.

ε_o = free space permittivity

μ_o = free space permeability

c = speed of light in a vacuum

ε_ℓ = relative lattice dielectric constant

ω_p = plasma frequency

ω_c = cyclotron frequency

Γ = propagation constant

τ = collision time

$$Z_o = \frac{1}{Y_o} = (\mu_o/\varepsilon_o)^{1/2}$$

$$k_o^2 = \omega^2\mu_o\varepsilon_o = \frac{\omega^2}{c^2}$$

$$K_+ = -\frac{j\omega_p^2\tau(j\omega\tau+1)}{\omega[(j\omega\tau+1)^2 + \omega_c^2\tau^2]}$$

$$K_X = \frac{-j\omega_p^2\omega_c\tau^2}{\omega[(j\omega\tau+1)^2 + \omega_c^2\tau^2]}$$

$$K = 1 - \frac{j\omega_p^2\tau}{\omega(j\omega\tau+1)}$$

$$K_\ell = \varepsilon_+ = k_1 - jk_x$$

$$K_r = \varepsilon_- = K_1 + jk_x$$

J_m = Bessel function of the first kind of order m

N_m = Bessel function of the second kind of order m

$$F_{mm}(x,y) = J_m(x)N_m(y) - N_m(x)J_m(y)$$

$$F_{mm'}(x,y) = \frac{\partial}{\partial y}F_{mm}(x,y)$$

$$F'_{mm}(x,y) = \frac{\partial}{\partial x}F_{mm}(x,y)$$

$$F'_{mm'}(x,y) = \frac{\partial}{\partial x}\,\frac{\partial}{\partial y}F_{mm}(x,y)$$

$$q^2 = \Gamma^2 + k_o^2$$

$$D = (\Gamma^2 + k_o^2 K_r)(\Gamma^2 + k_o^2 K_\ell)$$

$$P = -\Gamma(\Gamma^2 + k_o^2 K_\perp)/D$$

$$R = j\omega\mu_o k_o^2 K_x/D$$

$$Q = \Gamma k_o^2 K_x/D$$

$$S = j\omega\mu_o(\Gamma^2 + k_o^2 K_\perp)$$

$$a = (\Gamma^2 + k_o^2 K_\perp)K_{||}/K_\perp$$

$$b = j\omega\mu_o K_x/K_\perp$$

$$c = (\Gamma^2 + k_o^2)K_r K_\ell/K_\perp$$

$$d = j\omega\varepsilon_o K_x K_{||}/K_\perp$$

$$p_{1,2}^2 = \tfrac{1}{2}\Gamma^2(K_{||}/K_\perp + 1) + k_o^2(K_{||} + K_r K_\ell/K_\perp)$$

$$\pm\ \tfrac{1}{2}\Gamma^2(K_{||}/K_\perp - 1) + k_o^2(K_{||} - K_r K_\ell/K_\perp)^2$$

$$+\ 4\Gamma^2 k_o^2 K_{||}\ K_x^2/K_\perp^2$$

$$h_{1,2} = (a - p_{1,2}^2)/b$$

$$_{1,2} = p_{1,2}^2 R/b - 1/\Gamma$$

$$L_{1,2} = p_{1,2}^2 S/b - (1/\Gamma)(K_\perp/K_x)$$

$$y_{1,2} = (p_{1,2}^2 p + \Gamma)/b$$

$$Y_{1,2} = p_{1,2}^2 Q/b$$

$$\xi = -\Gamma^2/q^2$$

$$\zeta = jk_o/q$$

$$S_1(p_1 x) = \frac{jm}{x}\ell_2 J_m(p_1 x) + L_2 P_1 J_m'(p_1 x)$$

$$S_2(p_1 x) = \frac{jm}{x}\ell_2 N_m(p_1 x) + L_2 P_1 N_m'(p_1 x)$$

$$S_3(p_2 x) = \frac{jm}{x}\ell_1 J_m(p_2 x) + L_1 P_2 J_m'(p_2 x)$$

$$S_4(p_2 x) = \frac{jm}{x}\ell_1 N_m(p_2 x) + L_1 P_2 N_m'(p_2 x)$$

$$T_1(p_1 x) + \frac{jm}{x}y_2 J_m(p_1 x) + Y_2 P_1 J_m'(p_1 x)$$

$$T_2(p_1 x) + \frac{jm}{x}y_2 N_m(p_1 x) + Y_2 P_1 N_m'(p_1 x)$$

$$T_3(p_2 x) = \frac{jm}{x}y_1 J_m(p_2 x) + Y_1 P_2 J_m'(p_2 x)$$

$$T_4(p_2 x) + \frac{jm}{x}y_1 N_m(p_1 x) + Y_1 P_2 N_m'(p_2 x)$$

REFERENCES

1. Rau, R.R. and M.T. Caspari, "Faraday effect in germanium at room temperature", Phys. Rev., vol. 100, pp. 632-639, 1955.
2. Stephen, M.J. and A.B. Lidard, "The Faraday effect in semiconductors," J. Phys. Chem. Solids, vol. 9, pp. 43-47, 1958.
3. Furdyna, J.K. and S. Broersma, "Microwave Faraday effect in silicon and germanium," Phys. Rev., vol. 120, pp. 1995-2003, 1960.
4. Bouwknegt, A. and J. Volger, "Measurement of the free carrier Faraday effect in n-type germanium at microwave frequencies," Physica., vol. 30, pp. 113-123, 1964.
5. Mansfield, R. and M.R. Borst, "The microwave Faraday effect in indium antimonide," Brit. J. Appl. Phys., vol. 16, pp. 570-572, 1965.
6. Kuno, H.J. and W.D. Hershberger, "Observation of microwave Faraday rotation in a solid state plasma," Proc. IEEE (letters) vol. 54, pp. 978-979, 1966.
7. Kuno, H.J., "Solid State plasma waveguides:microwave propagation and Faraday effect," Ph.D. Thesis, University of Calif., Los Angeles, 1966.
8. Afinogenov, V.M., V.V. Migulin and V.I. Trifonov, "Singularity of the Faraday effect in n-InSb in the millimeter band", JETP vol. 1, pp. 299, 1966.

9. Furdyna, J. K., "Helicons, magnetoplasma edge, and Faraday rotation in solid state plasmas at microwave frequencies," Applied Optics, Vol. 6, No. 4, pp. 675-684, 1967.

10. McLeod, B. R., "Quasi-optical and waveguide applications of indium antimonide," Ph.D. Thesis, University of Colorado, Boulder, 1968.

11. Donovan, B., and J. Webster, "The theory of the Faraday effect in anisotropic semiconductors," Proc. Phys. Soc., vol. 79, pp. 46-57, 1962.

12. Champlin, K.S., "Microwave free carrier Faraday effect in semiconductors. Perturbation theory for guided waves," Physica, vol. 28, pp. 1143-1149, 1962.

13. Donovan, B., and J. Webster, "The theory of the Faraday effect in anisotropic semiconductors: application to n-type germanium," Proc. Phys. Soc., vol. 81, pp. 90-103, 1963.

14. Furdyna, J.K., and M.E. Browdwin, "Magnetic field dependence of free carrier absorption in semiconductors," Phys. Rev. vol 132, pp. 97-104, 1963.

15. Donovan, B. and T. Medcalf, "The inclusion of multiple reflections in the theory of the Faraday effect in semiconductors," Phys. letters, vol. 7, pp. 304-306, 1963.

16. Donovan, B. and T. Medcalf, "The inclusion of multiple reflections in the theory of the Faraday effect in semiconductors," Brit. J. Appl. Phys.,vol. 15, pp. 1139-1151, 1964.

17. Van der Pauw, L. J., "Method of measuring specific resistivity and Hall effect of discs of arbitrary shape," Phillips

Research Reports, vol. 13, pp. 1-9, Feb. 1958.

18. Hogan, C. L., "The ferromagnetic Faraday effect at microwave frequencies and its applications: the microwave gyrator, Bell Sys. tech. I, vol. 31, pp 1-31, Jan. 1952.

19. Hogan, C. L., "The ferromagnetic Faraday effect at microwave frequencies and its applications," Rev. Mod. Phys., vol. 25, pp. 253-263, Jan. 1953.

20. Goldstein, L., Lampert, M., and Heney, J., "Magneto-optics of an electron gas with guided microwaves," Phys. Rev., vol. 82, pp. 956-957, June 1951.

21. Goldstein, L., "Nonreciprocal electromagnetic wave propagation in ionized gaseous media," IRE Trans. on Microwave Theory and Tech., vol. MTT-6, pp. 19-29, Jan. 1958.

22. Toda, M., "Propagation in a solid-state plasma waveguide in a transverse magnetic field," J. Phys. Soc. Japan, Vol. 19, pp 1126-1130, Jul. 1964.

23. Toda, M., "A new isolator using a solid-state plasma waveguide," IEEE Trans. on Microwave Theory and Tech., Vol. MTT-13, pp. 126-127, Jan. 1965.

24. Kuno, H.J., and Hershberger, W.D., "Solid-state plasma controlled non-reciprocal microwave device" IEEE Trans. on Microwave Theory and Tech., Vol. MTT-15, pp. 57-58, Jan. 1967.

25. Kuno, H. J. and Hershberger, W.D., "Microwave Faraday effect and propagation in a circular solid-state plasma waveguide," IEEE Trans. on Microwave Theory and Tech., Vol. MTT-15, pp. 661-668, Dec. 1967.

26. Trivelpiece, A.W., "Slow wave propagation in plasma waveguides," California Inst. of Tech., Report 7, May 1958.

27. Granatstein, V. L., Schlesinger, S. P., and Vigants, A., "The open plasmaguide in extremes of magnetic field," IEEE Trans. AP-11, p. 489, 1963.

28. Alfredsson, L., "Investigation of backward-wave modes in plasma waveguides," Trans. Roy. Inst. Tech., pp. 233, Stockholm, 1964.

29. Carlile, R. N., "A backward wave surface mode in a plasma waveguide," J. Appl. Phys., vol. 35, p. 1384, 1964.

30. Leprince, P. and Pommier, J., "Surface wave in a plasma column: Dipolar Mode," Proc. IEE, Vol. 113, p. 588, Apr. 1966.

31. Clarricoats, P.J.B., "Propagation in isotropic plasma waveguides," Proc. IEE, Vol. 113, pp. 755-766, May 1966.

32. Granatstein, V. L. and Schlesinger, S.P., "Electromagnetic waves in parameter space for finite magneto-plasmas," J. Appl. Phys. vol. 35, p. 284b, 1964.

33. Agdur, B., "Note on the propagation of guided microwaves," Proc. of Symposium on Electronic Waveguides, p. 177, New York, Apr. 1958.

34. Bevc, V. and Everhart, T.T., "Fast wave propagation in plasma filled waveguides," J. Electronics and Control, Vol. 13, p. 185, 1962.

35. Allis, W. P., Buchsbaum, S.J. and Bers, A., Waves in anisotropic plasma, MIT Press, Cambridge, Mass., 1963.

36. Ramo, S., Winnery, J.R. and Van Puzer, T., _Fields and waves in communication electronics_, p. 448, Wiley, New York, 1965

37. Paik, S.F., "Backwave waves in annular plasma columns," J. Electronics and Control, Vol. 13, pp. 515-524, 1962.

38. Napoli, L.S., and Swartz, G.A., "Wave propagation in a tubular plasma," Phys. of Fluids, Vol. 6, pp. 918-924, July 1963.

39. Clarricoats, P.J.B., and Wong, J.S.L., "Dispersion characteristics of circular waveguide containing isotropic plasma," Proc. IEE, Vol. 111, p. 1087, June 1964.

40. Dennis, J.H., "A 10.6 micron four-part circulator using free carrier rotation in InSb," IEEE Journal of Quantum Electronics, Vol. 3, p. 416, October 1967.